

# ASYMPTOTIC STABILITY AND DIFFUSION-DRIVEN PATTERN FORMATION IN A PREDATOR-PREY SYSTEM WITH TWO CHEMICALS

GNANASEKARAN SHANMUGASUNDARAM, JITRAJ SAHA\*, OLUWOLE DANIEL MAKINDE,  
AND JOYDEV CHATTOPADHYAY

ABSTRACT. This work analyzes a predator–prey cross-diffusion system coupled with two chemical substances under homogeneous Neumann boundary conditions in a bounded domain  $\Omega \subset \mathbb{R}^n$  ( $n \geq 2$ ) with smooth boundary  $\partial\Omega$ . Under appropriate conditions on the model parameters, the global existence of classical solutions is established. Furthermore, by constructing a suitable Lyapunov functional, the asymptotic stability of the spatially homogeneous steady state is proved. The emergence of spatial patterns induced by diffusion-driven instability is also investigated. Owing to the complexity of the resulting four-equation system, the criteria for Turing bifurcation are derived numerically rather than analytically. Numerical simulations are performed to generate Turing bifurcation diagrams, illustrating the dynamical responses of the system to variations in the predation rate. These results provide new insights into the role of predation intensity in the formation of spatial patterns in predator–prey systems mediated by two chemical substances.

## 1. INTRODUCTION AND MOTIVATION

Predator–prey dynamics have long stood at the core of mathematical ecology, beginning with the pioneering works of Lotka [1] and Volterra [2], who established a theoretical framework for population interactions through coupled nonlinear differential equations. These nonlinear interactions in the predator-prey systems can give rise to rich spatiotemporal behaviors that demand rigorous mathematical analysis. One of the most remarkable manifestations of such dynamics is the emergence of Turing patterns [3], which arise in reaction–diffusion systems due to interactions between activator and inhibitor components with different diffusion rates. These mechanisms provide explanations for a wide range of biological patterns, including animal coat markings and tissue morphogenesis. Segel and Jackson [4] were among the first to recognize that Turing’s theory could be extended to ecological systems, thereby linking pattern formation theory with population dynamics.

Traditional models of ecological pattern formation often rely on self-diffusion and assume time-independent parameters. However, self-diffusion alone is not sufficient to generate or sustain spatial patterns [5, 6]. This limitation has motivated the inclusion of the concept of cross-diffusion, which describes the movement of one species being dependent on the concentration gradient of another species. Cross-diffusion has been widely studied [7, 8, 9, 10, 11, 12, 13] and is now recognized as a key mechanism driving spatial heterogeneity and pattern formation in ecological systems, including Lotka–Volterra-type models [14]. Recent advances in reaction–diffusion predator–prey models have highlighted the crucial roles of spatial heterogeneity, behavioral responses, and nonlinear dispersal mechanisms in shaping ecosystem stability and

---

2020 *Mathematics Subject Classification.* 35A01, 35A09, 35B36, 35B40, 37N25, 65N06.

\*Corresponding author.

pattern formation. A broad spectrum of model formulations including cross-diffusion, Allee effects, fear effects, harvesting, and time delays has been extensively investigated. These studies have established rigorous criteria for local and global stability, as well as for Hopf and Turing bifurcations, which give rise to complex spatiotemporal dynamics. In this context, we briefly review some recent contributions reported in the literature.

*Literature review* : Ranjit et al. [15] investigated a reaction–diffusion predator–prey model incorporating both self- and cross-diffusion. They derived conditions for local stability, instability, and global asymptotic stability, showing that cross-diffusion significantly modifies diffusion-driven instability thresholds and can induce Turing patterns even when classical diffusion cannot. Their numerical simulations further revealed rich spatial structures governed by parameters such as predator immunity, predation rate, and the half-saturation constant. Santu and Swarup [16] studied Hopf and Turing bifurcations in a predator–prey system with additional food supply for predators. They established analytical criteria for both temporal oscillations and diffusion-driven instability, and their numerical simulations confirmed the theoretical findings. Their results indicate that supplementary feeding can shift stability boundaries and, when properly regulated, suppress spatiotemporal chaos, thereby offering a potential ecological control mechanism. Qian and Jianhua [17] analyzed a predator–prey model with chemotaxis-driven movement. They showed that chemotactic sensitivity generalizes classical Turing instability conditions and significantly enlarges the parameter space for pattern formation, enabling the emergence of spatial structures that cannot occur under pure diffusion.

Tamko et al. [18] investigated the spatiotemporal dynamics of a hepatitis B virus model formulated within a predator–prey-type framework involving competitive and commensal interactions.

$$\begin{cases} u_t = d_1 \nabla^2 u + r - du - \beta uv, \\ w_t = d_2 \nabla^2 w + \beta uv - aw, \\ v_t = d_3 \nabla^2 v + \gamma w - \mu v, \end{cases}$$

Numerical simulations were used to demonstrate the resulting pattern formation. Santu et al. [19] investigated the two-species predator–prey reaction–diffusion model incorporating the provision of additional food to the predator.

$$\begin{cases} u_t = d_{11} \nabla^2 u + d_{12} \nabla^2 v + u(1 - \frac{u}{\gamma}) - \frac{uv}{1 + \alpha\xi + u}, \\ v_t = d_{21} \nabla^2 u + d_{22} \nabla^2 v + \frac{\beta(u + \xi)v}{1 + \alpha\xi + u} - \delta v. \end{cases}$$

To determine the conditions for Turing instability, a linear stability analysis together with the influence of cross-diffusion on system stability is studied to determine Turing. Furthermore, pattern formation was illustrated through numerical simulations using the finite difference method (FDM). Their results indicate that the availability of additional food plays a significant role in generating diverse spatial patterns. Yong et al. [20] examined the dynamical behavior of a diffusive predator–prey system with a Michaelis–Menten-type functional response and linear harvesting. The model is given by

$$\begin{cases} u_t = d_1 \nabla^2 u + u(1 - u) - \frac{awv}{u + v} - hu, \\ v_t = d_2 \nabla^2 v - dv + \frac{buv}{u + v}. \end{cases}$$

They derived the conditions for Turing instability and validated these conditions through numerical simulations. Various solution types were observed, including non-constant steady states, homogeneous periodic solutions, and inhomogeneous periodic solutions. Bhaskar et al. [21] studied a tri-trophic food web model

$$\begin{cases} u_{1t} = d_1 \nabla^2 u_1 + u_1 \left( 1 - u_1 - \frac{u_2}{1 + c_1 u_1} - \frac{u_3}{1 + c_2 u_1 + c_3 u_2} \right), \\ u_{2t} = d_2 \nabla^2 u_2 + u_2 \left( \frac{c_4 u_1}{1 + c_1 u_1} - c_5 - \frac{c_6 u_3}{1 + c_2 u_1 + c_3 u_2} \right), \\ u_{3t} = d_3 \nabla^2 u_3 + u_3^2 \left( c_7 - \frac{c_8}{1 + c_9 u_1 + c_{10} u_2} \right). \end{cases}$$

and derived conditions for diffusion-driven Turing instability, wave instability, and chaotic oscillations around the coexistence equilibrium, particularly under over-dependence on a specific food source. Numerical simulations revealed several non-Turing instabilities, including Hopf, wave, Hopf–Turing, and Hopf–wave bifurcations. It was observed that diffusion can suppress both regular and irregular spatiotemporal oscillations, thereby stabilizing the system. Using heat maps of Lyapunov exponents across a bi-parametric space, the authors showed that Turing patterns dominate near the Hopf–Turing bifurcation threshold, whereas Hopf patterns prevail farther from this region. They also concluded that high-amplitude oscillations associated with Hopf-type instabilities can be detrimental to spatially distributed populations. Gourav et al. [22] examined a reaction–diffusion predator–prey system incorporating fear effects and anti-predator behavioral responses. Using bifurcation analysis and stability theory, they derived conditions for Hopf bifurcation and pattern formation. Their simulations demonstrated a variety of stationary and oscillatory spatial patterns, including non-Turing structures, highlighting the crucial role of behavioral responses in shaping ecological complexity.

Recently, Shunjie et al. [23] investigated pattern formation in a generalized reaction–diffusion framework, emphasizing robustness and symmetry properties. They derived criteria for symmetric pattern generation and showed through simulations that domain geometry plays a significant role in determining spatial structures, indicating that pattern formation depends not only on system kinetics but also on spatial configuration. Lakpa et al. [24] extended the classical Rosenzweig–MacArthur model by incorporating prey harvesting and variable carrying capacity. They established sufficient conditions for equilibrium stability and Hopf bifurcation, demonstrating that increased harvesting may stabilize coexistence, whereas stronger interaction parameters can destabilize the system via limit cycle oscillations. Furthermore, they derived Turing instability conditions under cross-diffusion and reported the emergence of diverse stationary and spatiotemporal patterns, including chaotic attractors, for appropriate parameter choices.

Diffusive predator–prey model that incorporates the Allee effect in the predator population along with harvesting applied to both species was studied by Esita et al. [25].

$$\begin{cases} u_t = d_1 \nabla^2 u + ru \left( 1 - \frac{u}{k} \right) - \alpha uv - e_1 u, \\ v_t = d_2 \nabla^2 v + \beta uv \left( \frac{v}{c + v} \right) - mv - e_2 v. \end{cases}$$

They analyzed the stability and bifurcation behavior of the temporal system by considering the Allee effect and harvesting rates as control parameters. For the spatial model, it was shown that both the Allee effect and harvesting can destabilize the system. Instead of focusing on long-term dynamics, the authors emphasized short-term dynamics and demonstrated the emergence of rich spatial patterns. Gourav et al. [26] analyzed the following predator–prey model with hunting

cooperation and an additive Allee effect.

$$\begin{cases} u_t = d_{11}\nabla^2 u + d_{12}\nabla^2 v + u \left( 1 - u - \frac{\mu}{u + \eta} \right) - \frac{\alpha(1 + \beta v)uv}{\gamma + (1 + \beta v)u}, \\ v_t = d_{21}\nabla^2 u + d_{22}\nabla^2 v + \frac{\alpha(1 + \beta v)uv}{\gamma + (1 + \beta v)u} - \delta v, \end{cases}$$

They investigated both local and global bifurcation structures of the temporal model and established the stability of all equilibrium points. Additionally, extensive numerical simulations were conducted to examine cross-diffusion-driven instabilities near the coexistence equilibrium. Their findings demonstrate that species interactions under cross-diffusion can intensify instability and lead to the emergence of spatial patterns, highlighting the critical role of cross-diffusion in sustaining ecosystem diversity and structure.

Pallav et al. [27] examined a Bazykin-type predator–prey model incorporating the Allee effect in the prey population.

$$\begin{cases} u_t = d_1\nabla^2 u + u \left( 1 - u - \frac{\theta}{u + \delta} \right) - uv, \\ v_t = d_2\nabla^2 v + \alpha uv - \beta v - \gamma v^2, \end{cases}$$

The authors analyzed ten distinct subregions in the parameter space by varying two key parameters and discussed both strong and weak Allee effects. In particular, they showed that strong Allee effects can lead to the extinction of both species. Numerical simulations revealed both stationary and non-stationary spatial patterns in fragmented habitats, illustrating how habitat fragmentation influences spatiotemporal dynamics. Muhammad et al. [28] studied a spatially extended predator–prey model with ratio-dependent interactions.

$$\begin{cases} u_t = d_1\nabla^2 u + u(a - bu) - \frac{cuv}{mv + u}, \\ v_t = d_2\nabla^2 v - dv + \frac{fuv}{mv + u}, \end{cases}$$

They derived conditions for both Hopf and Turing bifurcations and identified four distinct regions in the parameter space: stable, Turing instability, Hopf instability, and Hopf–Turing instability. Using a positivity-preserving finite difference scheme, they demonstrated a variety of spatial patterns under different parameter regimes, ensuring numerical stability in the sense of von Neumann.

Very recently, Suvankar et al. [29] explored an eco-epidemic model in which an infectious disease affects the prey population, incorporating prey refuge and intra-specific competition among predators.

$$\begin{cases} u_t = d_1\nabla^2 u + ru \left( 1 - \frac{u + v}{k} \right) - \lambda uv - \frac{\alpha_1(1 - \rho)uw}{1 + bw + c(1 - \rho)u} - q_1 Eu, \\ v_t = d_2\nabla^2 v + \lambda uv - \frac{mvw}{a + v} - \mu v - q_2 Ev, \\ w_t = d_3\nabla^2 w + \frac{\alpha_2(1 - \rho)uw}{1 + bw + c(1 - \rho)u} + \frac{\theta vw}{a + v} - dw - \delta w^2. \end{cases}$$

The authors derived the conditions for Turing instability in the spatial system and observed both stationary and non-stationary patterns through numerical simulations. By computing the maximum Lyapunov exponent, they confirmed that the non-stationary patterns exhibit chaotic behavior. They further emphasized that controlling chaos is essential for maintaining ecosystem stability, avoiding unpredictable population fluctuations, and ensuring sustainability.

To achieve this, a time-delay feedback control strategy was implemented, successfully stabilizing the spatiotemporal chaos.

To the best of our knowledge, existing studies on pattern formation in predator–prey systems consider either self-diffusion or direct cross-diffusion between species. However, cross-diffusion mediated by self-produced chemical signals has received comparatively lesser attention. This aspect is crucial for understanding and modeling cross-diffusion systems driven by chemical interactions.

## 2. MATHEMATICAL MODEL

Chemically mediated movement plays a crucial role in shaping ecological interactions. Many organisms release diffusible substances, such as chemoattractants or chemorepellents that influence the movement and spatial organization of other species [30, 31]. These interactions naturally give rise to cross-diffusion effects and can induce Turing-type instabilities, transforming homogeneous steady states into complex spatial patterns such as spots, stripes, or patchy distributions. A biologically relevant example of such mechanisms is found in bacteria–bacteriophage systems [32, 33]. Bacterial species, including *Escherichia coli* and *Pseudomonas*, release autoinducers and metabolic by-products that can enhance bacteriophage replication and facilitate their spatial spread. Conversely, bacteriophages release inhibitory substances during infection and lysis, suppressing bacterial growth and dispersal. Similar chemically mediated interactions are observed in algae–zooplankton systems [34, 35], where algae produce dissolved organic carbon that promotes zooplankton growth, while zooplankton release kairomones that inhibit algal reproduction and movement.

Motivated by these observations, we consider a predator–prey system in which chemical signaling governs species movement. Specifically, prey individuals release signaling chemicals  $v_1$ , which attract predators, inducing directed movement (advection) of predator density  $u_1$  along the gradient of  $v_1$ . Conversely, predators emit chemicals  $v_2$  that prey detect and avoid, leading to a repulsion-driven flux in prey density  $u_2$ . Such chemically mediated interactions provide evolutionary advantages by enhancing predator foraging efficiency and improving prey survival through avoidance strategies. As a result, cross-diffusion naturally emerges from these chemotactic responses. The resulting system is therefore given by

$$\left\{ \begin{array}{ll} u_{1t} = \nabla \cdot (d_{11}\nabla u_1 + d_{12}\nabla v_1) + u_1(\mu_1 - \lambda_1 u_1 + \eta_1 u_2), & x \in \Omega, t > 0, \\ u_{2t} = \nabla \cdot (d_{21}\nabla u_2 - d_{22}\nabla v_2) + u_2(\mu_2 - \lambda_2 u_2 - \eta_2 u_1), & x \in \Omega, t > 0, \\ v_{1t} = d_3 \Delta v_1 + a_1 u_2 - b_1 v_1, & x \in \Omega, t > 0, \\ v_{2t} = d_4 \Delta v_2 + a_2 u_1 - b_2 v_2, & x \in \Omega, t > 0, \\ \frac{\partial u_1}{\partial \nu} = \frac{\partial u_2}{\partial \nu} = \frac{\partial v_1}{\partial \nu} = \frac{\partial v_2}{\partial \nu} = 0, & x \in \partial\Omega, t > 0, \\ u_1(x, 0) = u_{10}, u_2(x, 0) = u_{20}, v_1(x, 0) = v_{10}, v_2(x, 0) = v_{20}, & x \in \Omega, \end{array} \right. \quad (2.1)$$

in an open, bounded domain  $\Omega \subset \mathbb{R}^n$  with smooth boundary  $\partial\Omega$ . Here,  $\nu$  represents the unit outward normal on  $\partial\Omega$ . The unknown functions  $u_1 = u_1(x, t)$  and  $u_2 = u_2(x, t)$  describes the density of the population of predator and prey, respectively, and  $v_1 = v_1(x, t)$ ,  $v_2 = v_2(x, t)$  denotes the concentration of chemical attractants produced by prey and predator respectively. Here, the parameters  $d_{11}, d_{12}, d_{21}, d_{22}, d_3, d_4, \mu_1, \mu_2, \lambda_1, \lambda_2, \eta_1, \eta_2, a_1, a_2, b_1$  and  $b_2$  are positive constants and the initial data  $u_{10}, u_{20}, v_{10}$  and  $v_{20}$  are non-negative functions. The constants  $d_{11}, d_{21}, d_3$  and  $d_4$  are labeled as self diffusion coefficients, where as  $d_{12}$  and  $d_{22}$  are the cross

diffusion coefficients,  $\nabla \cdot (d_{12} \nabla v_1)$  denotes the directional predator movement towards the substance produced by the prey and the term  $-\nabla \cdot (d_{22} \nabla v_2)$  describes the directional prey movement away from the substance produced by the predator. The growth rates of predator and prey are labeled as  $\mu_1$  and  $\mu_2$  respectively. The constants  $\lambda_1, \lambda_2$  are known as the interaction between the species themselves and  $\eta_1, \eta_2$  represent the interaction between other species. The parameters  $a_1$  and  $a_2$  characterizes the production rates of the signals by the prey and predator,  $b_1$  and  $b_2$  characterizes the decay rate of the chemical attractants. We assume the following conditions to ensure the parabolicity of (2.1)

$$4d_{11}d_3 > d_{12}^2 \quad \text{and} \quad 4d_{21}d_4 > d_{22}^2. \quad (2.2)$$

Further, assume that the initial data  $u_{10}, u_{20}, v_{10}$  and  $v_{20}$  satisfy

$$\begin{cases} u_{10}, u_{20} \in C^0(\bar{\Omega}), & \text{with } u_{10}, u_{20} \geq 0 \text{ in } \Omega, \\ v_{10}, v_{20} \in \mathcal{W}^{1,\infty}(\Omega), & \text{with } v_{10}, v_{20} \geq 0 \text{ in } \Omega. \end{cases} \quad (2.3)$$

Motivated by the works discussed in Section 1, this article aims to establish the following results

- (1) Global existence and boundedness of classical solutions to (2.1).
- (2) Global asymptotic stability of the classical solutions to (2.1).
- (3) Turing pattern formation induced by the system.

The remainder of this paper is organized as follows. In Section 3, we present preliminary lemmas and establish the local existence of classical solutions. Section 4 is devoted to proving the boundedness and global existence of solutions to system (2.1). Stability analysis is carried out in Section 5. In Section 6, we investigate pattern formation arising from cross-diffusion-driven instability. Finally, Section 7 concludes the paper with a brief summary of the results.

The primary theorems that are perinatal for the considered system are stated as follows.

**Theorem 2.1.** *Let  $\Omega \subset \mathbb{R}^n$  ( $n \geq 2$ ) be a bounded domain with smooth boundary, and assume that (2.2) is satisfied. Then, for any nonnegative initial data  $(u_{10}, u_{20}, v_{10}, v_{20})$  fulfilling (2.3), the system (2.1) admits a unique classical solution  $(u_1, u_2, v_1, v_2)$ , which remains uniformly bounded, in the sense that for all  $t > 0$*

$$\|u_1(\cdot, t)\|_{\mathcal{L}^\infty(\Omega)} + \|u_2(\cdot, t)\|_{\mathcal{L}^\infty(\Omega)} + \|v_1(\cdot, t)\|_{\mathcal{W}^{1,\infty}(\Omega)} + \|v_2(\cdot, t)\|_{\mathcal{W}^{1,\infty}(\Omega)} \leq C,$$

where  $C > 0$  is a constant.

Let  $(u_1, u_2, v_1, v_2)$  be the classical solution of (2.1) and  $(u_1^e, u_2^e, v_1^e, v_2^e)$  be the equilibria of (2.1), satisfying the following system

$$\begin{cases} u_1^e(\mu_1 - \lambda_1 u_1^e + \eta_1 u_2^e) = 0, \\ u_2^e(\mu_2 - \lambda_2 u_2^e - \eta_2 u_1^e) = 0, \\ a_1 u_2^e - b_1 v_1^e = 0, \\ a_2 u_1^e - b_2 v_2^e = 0. \end{cases}$$

The system has four equilibria

$$(0, 0, 0, 0), \quad \left(0, \frac{\mu_2}{a_2}, \frac{a_1 \mu_2}{a_2 b_1}, 0\right), \quad \left(\frac{\mu_1}{a_1}, 0, 0, \frac{a_2 \mu_1}{a_1 b_2}\right), \quad (u_1^*, u_2^*, v_1^*, v_2^*).$$

The coexistence equilibrium point  $(u_1^*, u_2^*, v_1^*, v_2^*)$  is given by

$$u_1^* = \frac{a_2 \mu_1 + \eta_1 \mu_2}{a_1 a_2 + \eta_1 \eta_2}, \quad u_2^* = \frac{a_1 \mu_2 - \eta_2 \mu_1}{a_1 a_2 + \eta_1 \eta_2}, \quad v_1^* = \frac{a_1 (a_1 \mu_2 - \eta_2 \mu_1)}{b_1 (a_1 a_2 + \eta_1 \eta_2)}, \quad v_2^* = \frac{a_2 (a_2 \mu_1 + \eta_1 \mu_2)}{b_2 (a_1 a_2 + \eta_1 \eta_2)}$$

provided  $a_1\mu_2 > \eta_2\mu_1$ .

**Theorem 2.2.** *Suppose that the assumptions of Theorem 2.1 hold true and let  $\eta_2 < \frac{\mu_2 a_1}{\mu_1}$ . If the parameters satisfy the relations*

$$d_{12}^2 < \min \left\{ \frac{16d_{11}d_3b_1\eta_1a_2(a_1a_2 + \eta_1\eta_2)\|u_1\|_{\mathcal{L}^\infty(\Omega)}^2}{a_1^2\eta_2(a_2\mu_1 + \eta_1\mu_2)}, 4d_{11}d_3 \right\},$$

$$d_{22}^2 < \min \left\{ \frac{16d_{21}d_4b_2\eta_2a_1(a_1a_2 + \eta_1\eta_2)\|u_2\|_{\mathcal{L}^\infty(\Omega)}^2}{a_2^2\eta_1(a_1\mu_2 - \eta_2\mu_1)}, 4d_{21}d_4 \right\},$$

then the nonnegative classical solution  $(u_1, u_2, v_1, v_2)$  of the system (2.1) exponentially converges to the unique positive equilibrium point  $(u_1^*, u_2^*, v_1^*, v_2^*)$  uniformly in  $\Omega$  as  $t \rightarrow \infty$ .

**Theorem 2.3.** *Suppose that the assumptions of Theorem 2.1 hold true and let  $\eta_2 \geq \frac{\mu_2 a_1}{\mu_1}$ . If the parameters satisfy the relation*

$$d_{12}^2 < \min \left\{ \frac{16d_{11}d_3b_1\eta_1a_1a_2\|u_1\|_{\mathcal{L}^\infty(\Omega)}^2}{a_1^2\mu_1\eta_2}, 4d_{11}d_3 \right\},$$

then the nonnegative classical solution  $(u_1, u_2, v_1, v_2)$  of the system (2.1) converges to the semi-trivial equilibrium point  $\left(\frac{\mu_1}{a_1}, 0, 0, \frac{\mu_1 a_2}{a_1 b_2}\right)$  uniformly in  $\Omega$  as  $t \rightarrow \infty$ .

### 3. PRELIMINARIES AND LOCAL EXISTENCE OF SOLUTIONS

**Lemma 3.1** (Local Existence). *Let  $\Omega \subset \mathbb{R}^n$  ( $n \geq 2$ ) be a bounded domain with smooth boundary. Suppose the initial data  $u_{10}, u_{20}, v_{10}$ , and  $v_{20}$  satisfy (2.3) for some  $p > n$ , and assume that condition (2.2) holds. Then there exists a maximal time  $T_{\max} \in (0, \infty]$  for which the system (2.1) admits a unique solution  $(u_1, u_2, v_1, v_2)$  satisfying*

$$u_1, u_2 \in \mathcal{C}^0(\bar{\Omega} \times [0, T_{\max})) \cap \mathcal{C}^{2,1}(\bar{\Omega} \times (0, T_{\max})),$$

$$v_1, v_2 \in \mathcal{C}^0(\bar{\Omega} \times [0, T_{\max})) \cap \mathcal{C}^{2,1}(\bar{\Omega} \times (0, T_{\max})) \cap \mathcal{L}_{loc}^\infty([0, T_{\max}); \mathcal{W}^{1,p}(\Omega)).$$

Furthermore, either  $T_{\max} = \infty$  or

$$\lim_{t \rightarrow T_{\max}} \left( \|u_1\|_{\mathcal{L}^\infty(\Omega)} + \|u_2\|_{\mathcal{L}^\infty(\Omega)} + \|v_1\|_{\mathcal{W}^{1,p}(\Omega)} + \|v_2\|_{\mathcal{W}^{1,p}(\Omega)} \right) = \infty. \quad (3.1)$$

*Proof.* The standard arguments involving the quasi-linear parabolic theory is used to prove the lemma. Let  $w = (u_1, u_2, v_1, v_2)^T \in \mathbb{R}^4$ , then system (2.1) can be reformed as

$$\begin{cases} w_t = \nabla \cdot (\mathcal{A}\nabla w) + \mathcal{F}(w), & x \in \Omega, t > 0, \\ \frac{\partial w}{\partial \nu} = 0, & x \in \partial\Omega, t > 0, \\ w(x, 0) = w_0, & x \in \Omega, \end{cases}$$

where

$$\mathcal{A} = \begin{pmatrix} d_{11} & 0 & d_{12} & 0 \\ 0 & d_{21} & 0 & -d_{22} \\ 0 & 0 & d_3 & 0 \\ 0 & 0 & 0 & d_4 \end{pmatrix}, \quad \mathcal{F}(w) = \begin{pmatrix} u_1(\mu_1 - \lambda_1 u_1 + \eta_1 u_2) \\ u_2(\mu_2 - \lambda_2 u_2 - \eta_2 u_1) \\ a_1 u_2 - b_1 v_1 \\ a_2 u_1 - b_2 v_2 \end{pmatrix}.$$

Under the parabolicity condition stated in (2.2), Amann's theory (Theorem 14.4 in [36]) ensures the existence of a weak maximal solution. Moreover, by Theorem 14.6 in [36], this solution is in fact classical and satisfies (2.1) pointwise.

*Nonnegativity of the solution:* Define the negative parts  $u_i^- := \max\{-u_i, 0\}$  and  $v_i^- := \max\{-v_i, 0\}$  for  $i = 1, 2$ , and set  $\mathcal{N}(t) := \sum_{i=1}^2 \|u_i^-(\cdot, t)\|_{\mathcal{L}^2(\Omega)}^2 + \sum_{i=1}^2 \|v_i^-(\cdot, t)\|_{\mathcal{L}^2(\Omega)}^2$ . We multiply each equation of (2.1) by the negative part of the corresponding component and integrate over  $\Omega$ . Using the identity  $\int_{\Omega} (\nabla \cdot F) w^- = -\int_{\Omega} F \cdot \nabla w^-$  and the fact that  $\nabla w = -\nabla w^-$  on  $w < 0$ , we obtain the diffusion contributions

$$\begin{aligned} \int_{\Omega} \nabla \cdot (d_{11} \nabla u_1 + d_{12} \nabla v_1) u_1^- &= d_{11} \int_{\Omega} |\nabla u_1^-|^2 - d_{12} \int_{\Omega} \nabla v_1 \cdot \nabla u_1^-, \\ \int_{\Omega} \nabla \cdot (d_{21} \nabla u_2 - d_{22} \nabla v_2) u_2^- &= d_{21} \int_{\Omega} |\nabla u_2^-|^2 + d_{22} \int_{\Omega} \nabla v_2 \cdot \nabla u_2^-, \\ \int_{\Omega} d_3 \Delta v_1 v_1^- &= d_3 \int_{\Omega} |\nabla v_1^-|^2, \\ \int_{\Omega} d_4 \Delta v_2 v_2^- &= d_4 \int_{\Omega} |\nabla v_2^-|^2. \end{aligned}$$

Therefore, we get

$$\begin{aligned} \frac{1}{2} \frac{d}{dt} \mathcal{N}(t) + d_{11} \|\nabla u_1^-\|_{\mathcal{L}^2(\Omega)}^2 + d_{21} \|\nabla u_2^-\|_{\mathcal{L}^2(\Omega)}^2 + d_3 \|\nabla v_1^-\|_{\mathcal{L}^2(\Omega)}^2 + d_4 \|\nabla v_2^-\|_{\mathcal{L}^2(\Omega)}^2 \\ = d_{12} \int_{\Omega} \nabla v_1 \cdot \nabla u_1^- - d_{22} \int_{\Omega} \nabla v_2 \cdot \nabla u_2^- - \sum_{i=1}^4 \int_{\Omega} \mathcal{F}_i(w_i) w_i^-, \end{aligned} \quad (3.2)$$

where  $w_1^- = u_1^-$ ,  $w_2^- = u_2^-$ ,  $w_3^- = v_1^-$  and  $w_4^- = v_2^-$ . Applying Young's inequality, we get

$$\begin{aligned} \left| d_{12} \nabla v_1 \cdot \nabla u_1^- \right| &\leq \frac{d_{12}^2}{2d_3} |\nabla u_1^-|^2 + \frac{d_3}{2} |\nabla v_1^-|^2, \\ \left| d_{22} \nabla v_2 \cdot \nabla u_2^- \right| &\leq \frac{d_{22}^2}{2d_4} |\nabla u_2^-|^2 + \frac{d_4}{2} |\nabla v_2^-|^2. \end{aligned}$$

Using the structural assumptions  $4d_{11}d_3 > d_{12}^2$  and  $4d_{21}d_4 > d_{22}^2$ , we conclude that the coefficients  $d_{11} - \frac{d_{12}^2}{2d_3} > 0$  and  $d_{21} - \frac{d_{22}^2}{2d_4} > 0$ , and hence there exists  $c_1 > 0$  such that

$$d_{11} \|\nabla u_1^-\|_{\mathcal{L}^2(\Omega)}^2 + d_3 \|\nabla v_1^-\|_{\mathcal{L}^2(\Omega)}^2 - d_{12} \int_{\Omega} \nabla v_1 \cdot \nabla u_1^- \geq c_1 \left( \|\nabla u_1^-\|_{\mathcal{L}^2(\Omega)}^2 + \|\nabla v_1^-\|_{\mathcal{L}^2(\Omega)}^2 \right), \quad (3.3)$$

$$d_{21} \|\nabla u_2^-\|_{\mathcal{L}^2(\Omega)}^2 + d_4 \|\nabla v_2^-\|_{\mathcal{L}^2(\Omega)}^2 + d_{22} \int_{\Omega} \nabla v_2 \cdot \nabla u_2^- \geq c_1 \left( \|\nabla u_2^-\|_{\mathcal{L}^2(\Omega)}^2 + \|\nabla v_2^-\|_{\mathcal{L}^2(\Omega)}^2 \right). \quad (3.4)$$

Since the reaction vector  $\mathcal{F}_i(w_i)$  is quasi-positive and  $w = -w^-$  on  $w < 0$ , we get

$$-\mathcal{F}_1(u_1)u_1^- = -u_1(\mu_1 - \lambda_1 u_1 + \eta_1 u_2)u_1^- = (u_1^-)^2(\mu_1 - \lambda_1 u_1 + \eta_1 u_2) \leq (\mu_1 + \lambda_1 C_1 + \eta_1 C_2)(u_1^-)^2$$

here we using  $\|u_1\|, \|u_2\| \leq C$  from local existence. Similarly,

$$\begin{aligned} -\mathcal{F}_2(u_2)u_2^- &= \mu_2(u_2^-)^2 - \lambda_2 u_2(u_2^-)^2 - \eta_2 u_1(u_2^-)^2 \leq (\mu_2 + \lambda_2 C_3 + \eta_2 C_4)(u_2^-)^2, \\ -\mathcal{F}_3(v_1)v_1^- &= -a_1 u_2 v_1^- + b_1 v_1 v_1^- = a_1 u_2^- v_1^- - b_1 v_1^- v_1^- \leq a_1 u_2^- v_1^-, \\ -\mathcal{F}_4(v_2)v_2^- &= -a_2 u_1 v_2^- + b_2 v_2 v_2^- = a_2 u_1^- v_2^- - b_2 v_2^- v_2^- \leq a_2 u_1^- v_2^-. \end{aligned}$$

Combining all the terms and then applying Young's inequality to get

$$-\sum_{i=1}^4 \int_{\Omega} \mathcal{F}_i(w_i) w_i^- \leq \int_{\Omega} (\mu_1 + \lambda_1 C_1 + \eta_1 C_2)(u_1^-)^2 + \frac{a_2}{2} (u_1^-)^2 + \int_{\Omega} (\mu_2 + \lambda_2 C_3 + \eta_2 C_4)(u_2^-)^2$$

$$+ \frac{a_1}{2}(u_2^-)^2 + \int_{\Omega} \frac{a_1}{2}(v_1^-)^2 + \frac{a_2}{2}(v_2^-)^2 \quad (3.5)$$

Substitute (3.3)-(3.5) in to (3.2) yields

$$\frac{d}{dt}\mathcal{N}(t) + 2c_1 \sum_{i=1}^4 \|\nabla w_i^-\|_{\mathcal{L}^2(\Omega)}^2 \leq 2c_2 \mathcal{N}(t).$$

Dropping the nonnegative gradient term and applying Grönwall's inequality,  $\mathcal{N}(t) \leq \mathcal{N}(0)e^{2c_2 t}$ . Because the initial data are nonnegative,  $\mathcal{N}(0) = 0$ , hence  $\mathcal{N}(t) = 0$  for all  $t \geq 0$ . Therefore  $u_i^- = v_i^- \equiv 0$  and  $u_1, u_2, v_1, v_2 \geq 0$  in  $\Omega \times [0, \infty)$ .  $\square$

Let  $s_0 \in (0, T_{\max})$  be such that  $s_0 < 1$ . By Lemma 3.1, we have  $u_1(\cdot, s_0), u_2(\cdot, s_0), v_1(\cdot, s_0), v_2(\cdot, s_0) \in \mathcal{C}^2(\bar{\Omega})$  with  $\frac{\partial v_i(\cdot, s_0)}{\partial \nu} = 0, i = 1, 2$ . Choose a constant  $C > 0$  for which

$$\begin{aligned} \sup_{0 \leq s \leq s_0} \|u_1(\cdot, s)\|_{\mathcal{L}^\infty(\Omega)} &\leq C, & \sup_{0 \leq s \leq s_0} \|u_2(\cdot, s)\|_{\mathcal{L}^\infty(\Omega)} &\leq C, \\ \sup_{0 \leq s \leq s_0} \|v_1(\cdot, s)\|_{\mathcal{L}^\infty(\Omega)} &\leq C, & \|\Delta v_1(\cdot, s_0)\|_{\mathcal{L}^\infty(\Omega)} &\leq C, \\ \sup_{0 \leq s \leq s_0} \|v_2(\cdot, s)\|_{\mathcal{L}^\infty(\Omega)} &\leq C, & \|\Delta v_2(\cdot, s_0)\|_{\mathcal{L}^\infty(\Omega)} &\leq C. \end{aligned} \quad (3.6)$$

**Lemma 3.2** ([37]). *Let  $y$  be a positive absolutely continuous function on  $(0, \infty)$  that satisfies*

$$\begin{cases} y'(t) + Ay^p \leq B, \\ y(0) = y_0, \end{cases}$$

with some constants  $A > 0, B \geq 0$  and  $p \geq 1$ . Then for  $t > 0$ , we have

$$y(t) \leq \max \left\{ y_0, \left( \frac{B}{A} \right)^{\frac{1}{p}} \right\}.$$

**Lemma 3.3.** *The classical solution  $(u_1, u_2, v_1, v_2)$  of (2.1) satisfies*

$$\int_{\Omega} u_1 \leq M_1 := \max \left\{ \int_{\Omega} u_{10} + \frac{\eta_1}{\eta_2} \int_{\Omega} u_{20}, \frac{|\Omega|}{4} \left( \frac{(\mu_1 + 1)^2}{a_1} + \frac{\eta_1 (\mu_2 + 1)^2}{\eta_2 a_2} \right) \right\}, \quad (3.7)$$

$$\int_{\Omega} u_2 \leq M_2 := \max \left\{ \int_{\Omega} u_{20}, |\Omega| \right\}, \quad (3.8)$$

for all  $t \in (0, T_{\max})$ .

*Proof.* Proof of this lemma is similar to [38]. From second equation of (2.1), we see that

$$\frac{d}{dt} \int_{\Omega} u_2 \leq \mu_2 \int_{\Omega} u_2 - \lambda_2 \int_{\Omega} u_2^2.$$

Applying the Cauchy-Schwarz inequality,

$$\frac{d}{dt} \int_{\Omega} u_2 \leq \mu_2 \int_{\Omega} u_2 - \frac{\lambda_2}{|\Omega|} \left( \int_{\Omega} u_2 \right)^2,$$

by Lemma 3.2 yields (3.8). Subsequently, the first equation and  $\frac{\eta_1}{\eta_2}$  times the second equation of (2.1) are integrated and summed up on  $\Omega$  yields

$$\begin{aligned} \frac{d}{dt} \left( \int_{\Omega} u_1 + \int_{\Omega} \frac{\eta_1}{\eta_2} u_2 \right) &\leq \mu_1 \int_{\Omega} u_1 - \lambda_1 \int_{\Omega} u_1^2 + \eta_1 \int_{\Omega} u_1 u_2 + \frac{\eta_1 \mu_2}{\eta_2} \int_{\Omega} u_2 - \frac{\eta_1 \lambda_2}{\eta_2} \int_{\Omega} u_2^2 \\ &\quad - \eta_1 \int_{\Omega} u_1 u_2, \end{aligned}$$

Appending terms on both sides, we get

$$\begin{aligned} \frac{d}{dt} \left( \int_{\Omega} u_1 + \int_{\Omega} \frac{\eta_1}{\eta_2} u_2 \right) + \left( \int_{\Omega} u_1 + \int_{\Omega} \frac{\eta_1}{\eta_2} u_2 \right) &\leq (\mu_1 + 1) \int_{\Omega} u_1 - \lambda_1 \int_{\Omega} u_1^2 + \frac{\eta_1}{\eta_2} (\mu_2 + 1) \int_{\Omega} u_2 \\ &\quad - \frac{\eta_1 \lambda_2}{\eta_2} \int_{\Omega} u_2^2. \end{aligned}$$

Using the Cauchy's inequality, the equation takes the form

$$\frac{d}{dt} \left( \int_{\Omega} u_1 + \int_{\Omega} \frac{\eta_1}{\eta_2} u_2 \right) + \left( \int_{\Omega} u_1 + \int_{\Omega} \frac{\eta_1}{\eta_2} u_2 \right) \leq \frac{|\Omega|}{4} \left( \frac{(\mu_1 + 1)^2}{\lambda_1} + \frac{\eta_1}{\eta_2 \lambda_2} (\mu_2 + 1)^2 \right).$$

Set  $X(t) = \int_{\Omega} u_1 + \int_{\Omega} \frac{\eta_1}{\eta_2} u_2$ , the above inequality can be written as  $X'(t) + X(t) \leq C$ , where  $C = \frac{|\Omega|}{4} \left( \frac{(\mu_1 + 1)^2}{\lambda_1} + \frac{\eta_1}{\eta_2 \lambda_2} (\mu_2 + 1)^2 \right)$ . Utilizing the ODE argument Lemma 3.2, finally yields (3.7).  $\square$

**Lemma 3.4** (Maximal Sobolev regularity [39, 40]). *Let  $r \in (1, \infty)$  and  $T \in (0, \infty)$ . Consider the following evolution equation*

$$\begin{cases} y_t = \Delta y - y + g, & x \in \Omega, t > 0, \\ \frac{\partial y}{\partial \nu} = 0, & x \in \partial\Omega, t > 0, \\ y(x, 0) = y_0(x), & x \in \Omega. \end{cases}$$

For each  $y_0 \in \mathcal{W}^{2,r}(\Omega)$  ( $r > n$ ) with  $\frac{\partial y_0}{\partial \nu} = 0$  on  $\partial\Omega$  and any  $g \in \mathcal{L}^r((0, T); \mathcal{L}^r(\Omega))$ , there exists a unique solution

$$y \in \mathcal{W}^{1,r}((0, T); \mathcal{L}^r(\Omega)) \cap \mathcal{L}^r((0, T); \mathcal{W}^{2,r}(\Omega)).$$

Moreover, there exists  $C_r > 0$ , such that

$$\begin{aligned} \int_0^T \|y(\cdot, t)\|_{\mathcal{L}^r(\Omega)}^r dt + \int_0^T \|y_t(\cdot, t)\|_{\mathcal{L}^r(\Omega)}^r dt + \int_0^T \|\Delta y(\cdot, t)\|_{\mathcal{L}^r(\Omega)}^r dt \\ \leq C_r \int_0^T \|g(\cdot, t)\|_{\mathcal{L}^r(\Omega)}^r dt + C_r \|y_0\|_{\mathcal{L}^r(\Omega)}^r + C_r \|\Delta y_0\|_{\mathcal{L}^r(\Omega)}^r. \end{aligned}$$

If  $s_0 \in [0, T)$  and  $y(\cdot, s_0) \in \mathcal{W}^{2,r}(\Omega)$  ( $r > n$ ) with  $\frac{\partial y(\cdot, s_0)}{\partial \nu} = 0$  on  $\partial\Omega$ , then

$$\int_{s_0}^T e^{sr} \|\Delta y(\cdot, t)\|_{\mathcal{L}^r(\Omega)}^r dt \leq C_r \int_{s_0}^T e^{sr} \|g(\cdot, t)\|_{\mathcal{L}^r(\Omega)}^r dt + C_r \|y(\cdot, s_0)\|_{\mathcal{L}^r(\Omega)}^r + C_r \|\Delta y(\cdot, s_0)\|_{\mathcal{L}^r(\Omega)}^r.$$

Next we prove the main result of our problem (2.1).

#### 4. GLOBAL EXISTENCE OF SOLUTIONS

This section is dedicated to demonstrating the global existence and boundedness of the solution to (2.1). First we derive  $\mathcal{L}^q(\Omega)$  bound for  $u_1$  and  $u_2$ ,  $t \in (s_0, T_{\max})$ .

**Lemma 4.1.** *Suppose that  $\Omega \subset \mathbb{R}^n$  ( $n \geq 2$ ) is a bounded domain with smooth boundary. Assume that for any  $q > 1$ , there exists  $\lambda(q, d_{12}, d_{22}, a_1, a_2, \eta_1) > 0$ , such that if  $\lambda < \min \left\{ \frac{\lambda_1}{2}, \frac{\lambda_2}{2} \right\}$ , then*

$$\|u_1\|_{\mathcal{L}^q(\Omega)} + \|u_2\|_{\mathcal{L}^q(\Omega)} \leq C, \quad \forall t \in (0, T_{\max}),$$

for some  $C > 0$ .

*Proof.* Multiplying the first equation of (2.1) by  $u_1^{q-1}$ ,  $q > 1$  and integrating over  $\Omega$ , we get

$$\int_{\Omega} u_1 u_1^{q-1} = d_{11} \int_{\Omega} u_1^{q-1} \Delta u_1 + d_{12} \int_{\Omega} u_1^{q-1} \Delta v_1 + \int_{\Omega} u_1^{q-1} u_1 (\mu_1 - \lambda_1 u_1 + \eta_1 u_2).$$

Applying the technique of integration by parts,

$$\begin{aligned} \frac{1}{q} \frac{d}{dt} \int_{\Omega} u_1^q &= -d_1(q-1) \int_{\Omega} u_1^{q-2} |\nabla u_1|^2 + d_{12} \int_{\Omega} u_1^{q-1} \Delta v_1 + \mu_1 \int_{\Omega} u_1^q \\ &\quad - \lambda_1 \int_{\Omega} u_1^{q+1} + \eta_1 \int_{\Omega} u_1^q u_2. \end{aligned} \quad (4.1)$$

Utilizing the Gagliardo-Nirenberg inequality and the Young's inequality, it follows that

$$\begin{aligned} \int_{\Omega} u_1^q &= \left\| u_1^{\frac{q}{2}} \right\|_{\mathcal{L}^2(\Omega)}^2 \leq c'_1 \left( \left\| \nabla u_1^{\frac{q}{2}} \right\|_{\mathcal{L}^2(\Omega)}^{2b} \left\| u_1^{\frac{q}{2}} \right\|_{\mathcal{L}^{\frac{2}{q}}(\Omega)}^{2(1-b)} + \left\| u_1^{\frac{q}{2}} \right\|_{\mathcal{L}^{\frac{2}{q}}(\Omega)}^2 \right) \\ &\leq \frac{4d_1(q-1)}{q(q+1)} \left( \left\| \nabla u_1^{\frac{q}{2}} \right\|_{\mathcal{L}^2(\Omega)}^{2b} \right)^{\frac{1}{b}} + c'_2 \left( \left\| u_1^{\frac{q}{2}} \right\|_{\mathcal{L}^{\frac{2}{q}}(\Omega)}^{2(1-b)} \right)^{\frac{1}{1-b}} + c'_1 \left\| u_1^{\frac{q}{2}} \right\|_{\mathcal{L}^{\frac{2}{q}}(\Omega)}^2 \\ &\leq \frac{4d_1(q-1)}{q(q+1)} \left\| \nabla u_1^{\frac{q}{2}} \right\|_{\mathcal{L}^2(\Omega)}^2 + c'_3 \|u_1\|_{\mathcal{L}^1(\Omega)}^q \\ &\leq \frac{4d_1(q-1)}{q(q+1)} \frac{q^2}{4} \int_{\Omega} u_1^{q-2} |\nabla u_1|^2 + c'_3 M_1^q. \end{aligned}$$

Hence we obtain

$$\frac{q+1}{q} \int_{\Omega} u_1^q \leq d_1(q-1) \int_{\Omega} u_1^{q-2} |\nabla u_1|^2 + c_1, \quad (4.2)$$

with  $c_1 > 0$ , where  $b = \frac{\frac{q}{2} - \frac{1}{2}}{\frac{q}{2} + \frac{1}{n} - \frac{1}{2}} \in (0, 1)$ . Now we rewrite the above equation (4.2) as follows

$$-d_1(q-1) \int_{\Omega} u_1^{q-2} |\nabla u_1|^2 \leq -\frac{q+1}{q} \int_{\Omega} u_1^q + c_1. \quad (4.3)$$

Using Young's inequality two times to the second term in (4.1), we get

$$d_{12} \int_{\Omega} u_1^{q-1} \Delta v_1 \leq \frac{\lambda_1}{6} \int_{\Omega} u_1^{q+1} + c'_4 \int_{\Omega} |\Delta v_1|^{\frac{q+1}{2}} \leq \frac{\lambda_1}{6} \int_{\Omega} u_1^{q+1} + c'_5 \int_{\Omega} |\Delta v_1|^{q+1} + c_2. \quad (4.4)$$

where  $c_2 > 0$ . Again, using the Young's inequality to the third term in (4.1), we obtain

$$\mu_1 \int_{\Omega} u_1^q \leq \frac{\lambda_1}{6} \int_{\Omega} u_1^{q+1} + c_3, \quad (4.5)$$

where  $c_3 > 0$ , and for fifth term in (4.1) as follows

$$\int_{\Omega} \eta_1 u_1^q u_2 \leq \frac{\lambda_1}{6} \int_{\Omega} u_1^{q+1} + c_4 \int_{\Omega} u_2^{q+1}, \quad (4.6)$$

with  $c_4 > 0$ . Substituting (4.3) - (4.6) in (4.1), we see that

$$\frac{d}{dt} \left( \frac{1}{q} \int_{\Omega} u_1^q \right) + (q+1) \left( \frac{1}{q} \int_{\Omega} u_1^q \right) \leq -\frac{\lambda_1}{2} \int_{\Omega} u_1^{q+1} + c'_5 \int_{\Omega} |\Delta v_1|^{q+1} + c_4 \int_{\Omega} u_2^{q+1} + c_5.$$

Adopting the variation of constants formula, we get

$$\begin{aligned} \frac{1}{q} \int_{\Omega} u_1^q &\leq -\frac{\lambda_1}{2} \int_{s_0}^t \int_{\Omega} e^{-(q+1)(t-s)} u_1^{q+1} + c'_5 \int_{s_0}^t \int_{\Omega} e^{-(q+1)(t-s)} |\Delta v_1|^{q+1} \\ &\quad + c_4 \int_{s_0}^t \int_{\Omega} e^{-(q+1)(t-s)} u_2^{q+1} + c_6, \end{aligned} \quad (4.7)$$

where  $c_6 > 0$ . According to Lemma 3.4, there exists  $c_7 > 0$  such that

$$\begin{aligned} c'_5 \int_{s_0}^t \int_{\Omega} e^{-(q+1)(t-s)} |\Delta v_1|^{q+1} &\leq c_7 \int_{s_0}^t \int_{\Omega} e^{-(q+1)(t-s)} u_2^{q+1} \\ &+ c_7 \|v_1(\cdot, s_0)\|_{\mathcal{L}^{q+1}(\Omega)}^{q+1} + c_7 \|\Delta v_1(\cdot, s_0)\|_{\mathcal{L}^{q+1}(\Omega)}^{q+1}. \end{aligned} \quad (4.8)$$

Substituting the last inequality (4.8) into (4.7), we arrive at

$$\frac{1}{q} \int_{\Omega} u_1^q \leq -\frac{\lambda_1}{2} \int_{s_0}^t \int_{\Omega} e^{-(q+1)(t-s)} u_1^{q+1} + c_8 \int_{s_0}^t \int_{\Omega} e^{-(q+1)(t-s)} u_2^{q+1} + c_9, \quad (4.9)$$

where,  $c_9 > 0$ . Similarly, we estimate for  $u_2$  as

$$\frac{1}{q} \int_{\Omega} u_2^q \leq -\frac{\lambda_2}{2} \int_{s_0}^t \int_{\Omega} e^{-(q+1)(t-s)} u_2^{q+1} + c_{10} \int_{s_0}^t \int_{\Omega} e^{-(q+1)(t-s)} u_1^{q+1} + c_{11}, \quad (4.10)$$

where the constant  $c_{11} > 0$ . Adding (4.9) and (4.10) affords us

$$\begin{aligned} \frac{1}{q} \left( \int_{\Omega} u_1^q + \int_{\Omega} u_2^q \right) &\leq -\left( \frac{\lambda_1}{2} - c_{10} \right) \int_{s_0}^t \int_{\Omega} e^{-(q+1)(t-s)} u_1^{q+1} \\ &- \left( \frac{\lambda_2}{2} - c_8 \right) \int_{s_0}^t \int_{\Omega} e^{-(q+1)(t-s)} u_2^{q+1} + c_{12}. \end{aligned} \quad (4.11)$$

Let  $\lambda = \max\{c_8, c_{10}\}$  such that  $0 < \lambda < \min\left\{\frac{\lambda_1}{2}, \frac{\lambda_2}{2}\right\}$ . Hence, we deduce from (4.11) that

$$\int_{\Omega} u_1^q + \int_{\Omega} u_2^q \leq c_{12}, \quad \forall t \in (0, T_{\max}),$$

where the constant  $c_{12} > 0$ . In view of (3.6), the proof is complete.  $\square$

**Proof of Theorem 2.1.** Assume that  $T_{\max} < \infty$ . The result follows from the standard parabolic regularity (Ladyzhenskaya et al. [41], Amann [42]) applied to the third equation in (2.1),

$$v_{1t} - d_3 \Delta v_1 + b_1 v_1 = a_1 u_2$$

which ensures the boundedness and regularity of  $v_1$ , provided that  $u_2$  satisfies the  $\mathcal{L}^q(\Omega)$ -bound obtained in Lemma 4.1, and similar procedure for  $v_2$ . Hence, there exists a constant  $C_1 > 0$  such that

$$\|v_1\|_{\mathcal{W}^{1,\infty}(\Omega)} + \|v_2\|_{\mathcal{W}^{1,\infty}(\Omega)} \leq C_1, \quad \forall t \in (0, T_{\max}). \quad (4.12)$$

Finally, one can employ the well-known Moser-Alikakos iteration technique ([43] Lemma A.1) with Lemma 4.1 to prove that there exists  $C_2 > 0$  fulfilling

$$\|u_1\|_{\mathcal{L}^\infty(\Omega)} + \|u_2\|_{\mathcal{L}^\infty(\Omega)} \leq C_2, \quad \forall t \in (0, T_{\max}).$$

This bound contradicts (3.1). Hence, it follows that  $T_{\max} = \infty$ . The proof is complete.

## 5. GLOBAL ASYMPTOTIC STABILITY

In this section, we examine the global asymptotic behaviour of solutions and equilibrium convergence rates to the system (2.1), utilizing the Lyapunov functional. The proof of these asymptotic behavior outcomes takes inspiration from the research presented in [44]. The following lemma's proof is derived from [45] and [46].

**Lemma 5.1.** *Let  $(u_1, u_2, v_1, v_2)$  be the nonnegative classical solution of the system (2.1) and suppose that the assumptions of Theorem 2.1 hold true. Then there exists  $\theta \in (0, 1)$  and  $C > 0$  such that*

$$\|u_1\|_{C^{2+\theta, 1+\frac{\theta}{2}}(\bar{\Omega} \times [t, t+1])} + \|u_2\|_{C^{2+\theta, 1+\frac{\theta}{2}}(\bar{\Omega} \times [t, t+1])} \leq C$$

and

$$\|v_1\|_{C^{2+\theta, 1+\frac{\theta}{2}}(\bar{\Omega} \times [t, t+1])} + \|v_2\|_{C^{2+\theta, 1+\frac{\theta}{2}}(\bar{\Omega} \times [t, t+1])} \leq C,$$

for all  $t \geq 1$ .

*Proof.* The proof is based on the standard parabolic regularity theory in [41] and Theorem 2.1. For more details see, [47, 48]  $\square$

**Lemma 5.2** ([44]). *Suppose that  $f : (1, \infty)$  is a uniformly continuous nonnegative function such that*

$$\int_1^\infty f(t) dt < \infty.$$

Then,  $f(t) \rightarrow 0$  as  $t \rightarrow \infty$ .

First we start with the coexistent state of the species.

**5.1. Coexistence state of the species.** Here we assume that  $\eta_2 < \frac{\mu_2 \lambda_1}{\mu_1}$  and

$$d_{12}^2 < \frac{16d_{11}d_3b_1\eta_1\lambda_2(\lambda_1\lambda_2 + \eta_1\eta_2)\|u_1\|_{\mathcal{L}^\infty(\Omega)}^2}{a_1^2\eta_2(\lambda_2\mu_1 + \eta_1\mu_2)}, \quad d_{22}^2 < \frac{16d_{21}d_4b_2\eta_2\lambda_1(\lambda_1\lambda_2 + \eta_1\eta_2)\|u_2\|_{\mathcal{L}^\infty(\Omega)}^2}{a_2^2\eta_1(\lambda_1\mu_2 - \eta_2\mu_1)}$$

hold. Let  $(u_1, u_2, v_1, v_2)$  be the classical solution of (2.1) satisfying (2.3) and  $(u_1^*, u_2^*, v_1^*, v_2^*)$  be the unique positive equilibrium point of the system (2.1).

**Lemma 5.3.** *There exist  $\delta_1, \delta_2 > 0$  and  $\epsilon_1 > 0$  such that the functions*

$$\begin{aligned} \mathcal{E}_1(t) &= \int_{\Omega} \left( u_1 - u_1^* - u_1^* \ln \frac{u_1}{u_1^*} \right) + \frac{\eta_1}{\eta_2} \int_{\Omega} \left( u_2 - u_2^* - u_2^* \ln \frac{u_2}{u_2^*} \right) + \frac{\delta_1}{2} \int_{\Omega} (v_1 - v_1^*)^2 \\ &\quad + \frac{\delta_2}{2} \int_{\Omega} (v_2 - v_2^*)^2 \end{aligned}$$

and

$$f_1(t) = \int_{\Omega} (u_1 - u_1^*)^2 + \int_{\Omega} (u_2 - u_2^*)^2 + \int_{\Omega} (v_1 - v_1^*)^2 + \int_{\Omega} (v_2 - v_2^*)^2$$

satisfy

$$\frac{d}{dt} \mathcal{E}_1(t) \leq -\epsilon_1 f_1(t), \quad t > 0. \quad (5.1)$$

where  $\epsilon_1 > 0$ .

*Proof.* Choose  $\Gamma_1 \in (0, \lambda_2)$ ,  $\Gamma_2 \in (0, \lambda_1)$  and fix  $\delta_1 \in \left( \frac{d_{12}^2 u_1^*}{4d_{11}d_3\|u_1\|_{\mathcal{L}^\infty(\Omega)}^2}, \frac{4b_1\eta_1\lambda_2}{a_1^2\eta_2} \right)$ ,

$\delta_2 \in \left( \frac{d_{22}^2 u_2^* \eta_1}{4d_{21}d_4\eta_2\|u_2\|_{\mathcal{L}^\infty(\Omega)}^2}, \frac{4b_2a_1}{a_2^2} \right)$ . Let us consider the energy of the system as follows

$$\mathcal{E}_1(t) = \mathcal{A}_1(t) + \frac{\eta_1}{\eta_2} \mathcal{B}_1(t) + \mathcal{C}_1(t) + \mathcal{D}_1(t), \quad t > 0,$$

Now, let  $\mathcal{H}(u) = u - u^e \ln u$ , for  $u > 0$ . Using the Taylor's formula, we have

$$\mathcal{H}(u) = \mathcal{H}(u^e) + \mathcal{H}'(u^e)(u - u^e) + \frac{1}{2}\mathcal{H}''(u^e)(u - u^e)^2 = \frac{1}{2u^e}(u - u^e)^2 \geq 0.$$

Therefore, we have  $\mathcal{A}_1(t) = \int_{\Omega} \mathcal{H}(u_1) - \mathcal{H}(u_1^e) \geq 0$ . Similarly, we can obtain  $\mathcal{B}_1(t) \geq 0$  and  $\mathcal{C}_1(t), \mathcal{D}_1(t) \geq 0$  by the nonnegativity of  $\delta_i, i = 1, 2$ .

Now, we can compute

$$\begin{aligned} \frac{d}{dt} \mathcal{A}_1(t) &= -d_{11}u_1^* \int_{\Omega} \left| \frac{\nabla u_1}{u_1} \right|^2 - d_{12}u_1^* \int_{\Omega} \frac{\nabla u_1}{u_1^2} \cdot \nabla v_1 + \int_{\Omega} (u_1 - u_1^*)(\mu_1 - \lambda_1 u_1 + \eta_1 u_2) \\ &= -d_{11}u_1^* \int_{\Omega} \left| \frac{\nabla u_1}{u_1} \right|^2 - d_{12}u_1^* \int_{\Omega} \frac{\nabla u_1}{u_1^2} \cdot \nabla v_1 \\ &\quad + \int_{\Omega} (u_1 - u_1^*) \left( \mu_1 - \lambda_1 u_1 + \eta_1 u_2 - (\mu_1 - \lambda_1 u_1^* + \eta_1 u_2^*) \right) \\ &= -d_{11}u_1^* \int_{\Omega} \left| \frac{\nabla u_1}{u_1} \right|^2 - d_{12}u_1^* \int_{\Omega} \frac{\nabla u_1}{u_1^2} \cdot \nabla v_1 - \lambda_1 \int_{\Omega} (u_1 - u_1^*)^2 \\ &\quad + \eta_1 \int_{\Omega} (u_1 - u_1^*)(u_2 - u_2^*). \end{aligned}$$

Analogously, for  $\mathcal{B}_1(t)$ ,

$$\begin{aligned} \frac{d}{dt} \mathcal{B}_1(t) &= -d_{21}u_2^* \int_{\Omega} \left| \frac{\nabla u_2}{u_2} \right|^2 - d_{22}u_2^* \int_{\Omega} \frac{\nabla u_2}{u_2^2} \cdot \nabla v_2 + \int_{\Omega} (u_2 - u_2^*)(\mu_2 - \lambda_2 u_2 - \eta_2 u_1) \\ &= -d_{21}u_2^* \int_{\Omega} \left| \frac{\nabla u_2}{u_2} \right|^2 - d_{22}u_2^* \int_{\Omega} \frac{\nabla u_2}{u_2^2} \cdot \nabla v_2 \\ &\quad + \int_{\Omega} (u_2 - u_2^*) \left( \mu_2 - \lambda_2 u_2 - \eta_2 u_1 - (\mu_2 - \lambda_2 u_2^* - \eta_2 u_1^*) \right) \\ &= -d_{21}u_2^* \int_{\Omega} \left| \frac{\nabla u_2}{u_2} \right|^2 - d_{22}u_2^* \int_{\Omega} \frac{\nabla u_2}{u_2^2} \cdot \nabla v_2 - \lambda_2 \int_{\Omega} (u_2 - u_2^*)^2 \\ &\quad - \eta_2 \int_{\Omega} (u_1 - u_1^*)(u_2 - u_2^*). \end{aligned}$$

Let us now consider

$$\begin{aligned} \frac{d}{dt} \mathcal{C}_1(t) &= -d_3 \delta_1 \int_{\Omega} |\nabla v_1|^2 + a_1 \delta_1 \int_{\Omega} (v_1 - v_1^*)u_2 + a_1 \delta_1 \int_{\Omega} (v_1 - v_1^*)u_2^* - a_1 \delta_1 \int_{\Omega} (v_1 - v_1^*)u_2^* \\ &\quad - b_1 \delta_1 \int_{\Omega} (v_1 - v_1^*)v_1 + b_1 \delta_1 \int_{\Omega} (v_1 - v_1^*)v_1^* - b_1 \delta_1 \int_{\Omega} (v_1 - v_1^*)v_1^* \\ &= -d_3 \delta_1 \int_{\Omega} |\nabla v_1|^2 + a_1 \delta_1 \int_{\Omega} (v_1 - v_1^*)(u_2 - u_2^*) - b_1 \delta_1 \int_{\Omega} (v_1 - v_1^*)(v_1 - v_1^*) \\ &\quad + \delta_1 \int_{\Omega} (v_1 - v_1^*)(a_1 u_2^* - b_1 v_1^*) \\ &= -d_3 \delta_1 \int_{\Omega} |\nabla v_1|^2 + a_1 \delta_1 \int_{\Omega} (v_1 - v_1^*)(u_2 - u_2^*) - b_1 \delta_1 \int_{\Omega} (v_1 - v_1^*)^2. \end{aligned}$$

By the similar way, we obtain

$$\frac{d}{dt} \mathcal{D}_1(t) = -d_4 \delta_2 \int_{\Omega} |\nabla v_2|^2 + a_2 \delta_2 \int_{\Omega} (v_2 - v_2^*)(u_1 - u_1^*) - b_2 \delta_2 \int_{\Omega} (v_2 - v_2^*)^2.$$

Combining all the terms, we get

$$\begin{aligned}
 \frac{d}{dt} \mathcal{E}_1(t) = & -d_{11}u_1^* \int_{\Omega} \left| \frac{\nabla u_1}{u_1} \right|^2 - d_{12}u_1^* \int_{\Omega} \frac{\nabla u_1}{u_1^2} \cdot \nabla v_1 - \lambda_1 \int_{\Omega} (u_1 - u_1^*)^2 \\
 & + \eta_1 \int_{\Omega} (u_1 - u_1^*)(u_2 - u_2^*) - d_{21} \frac{\eta_1}{\eta_2} u_2^* \int_{\Omega} \left| \frac{\nabla u_2}{u_2} \right|^2 - d_{22} \frac{\eta_1}{\eta_2} u_2^* \int_{\Omega} \frac{\nabla u_2}{u_2^2} \cdot \nabla v_2 \\
 & - \frac{\eta_1 \lambda_2}{\eta_2} \int_{\Omega} (u_2 - u_2^*)^2 - \eta_1 \int_{\Omega} (u_1 - u_1^*)(u_2 - u_2^*) - d_3 \delta_1 \int_{\Omega} |\nabla v_1|^2 \\
 & + a_1 \delta_1 \int_{\Omega} (v_1 - v_1^*)(u_2 - u_2^*) - b_1 \delta_1 \int_{\Omega} (v_1 - v_1^*)^2 - d_4 \delta_2 \int_{\Omega} |\nabla v_2|^2 \\
 & + a_2 \delta_2 \int_{\Omega} (v_2 - v_2^*)(u_1 - u_1^*) - b_2 \delta_2 \int_{\Omega} (v_2 - v_2^*)^2.
 \end{aligned} \tag{5.2}$$

Hence, by the Cauchy's inequality, we have acquired the following estimates

$$-d_{12}u_1^* \int_{\Omega} \frac{\nabla u_1}{u_1} \cdot \frac{\nabla v_1}{u_1} \leq d_{11}u_1^* \int_{\Omega} \left| \frac{\nabla u_1}{u_1} \right|^2 + \frac{d_{12}^2 u_1^*}{4d_{11} \|u_1\|_{\mathcal{L}^\infty(\Omega)}^2} \int_{\Omega} |\nabla v_1|^2, \tag{5.3}$$

$$-d_{22} \frac{\eta_1}{\eta_2} u_2^* \int_{\Omega} \frac{\nabla u_2}{u_2} \cdot \frac{\nabla v_2}{u_2} \leq d_{21} \frac{\eta_1}{\eta_2} u_2^* \int_{\Omega} \left| \frac{\nabla u_2}{u_2} \right|^2 + \frac{d_{22}^2 \eta_1 u_2^*}{4d_{21} \eta_2 \|u_2\|_{\mathcal{L}^\infty(\Omega)}^2} \int_{\Omega} |\nabla v_2|^2, \tag{5.4}$$

$$a_1 \delta_1 \int_{\Omega} (v_1 - v_1^*)(u_2 - u_2^*) \leq \Gamma_1 \frac{\eta_1}{\eta_2} \int_{\Omega} (u_2 - u_2^*)^2 + \frac{a_1^2 \delta_1^2 \eta_2}{4\Gamma_1 \eta_1} \int_{\Omega} (v_1 - v_1^*)^2, \tag{5.5}$$

$$a_2 \delta_2 \int_{\Omega} (v_2 - v_2^*)(u_1 - u_1^*) \leq \Gamma_2 \int_{\Omega} (u_1 - u_1^*)^2 + \frac{a_2^2 \delta_2^2}{4\Gamma_2} \int_{\Omega} (v_2 - v_2^*)^2. \tag{5.6}$$

Substituting the above estimates (5.3)-(5.6) in (5.2), we obtain

$$\begin{aligned}
 \frac{d}{dt} \mathcal{E}_1(t) \leq & \frac{d_{12}^2 u_1^*}{4d_{11} \|u_1\|_{\mathcal{L}^\infty(\Omega)}^2} \int_{\Omega} |\nabla v_1|^2 - \lambda_1 \int_{\Omega} (u_1 - u_1^*)^2 + \frac{d_{22}^2 \eta_1 u_2^*}{4d_{21} \eta_2 \|u_2\|_{\mathcal{L}^\infty(\Omega)}^2} \int_{\Omega} |\nabla v_2|^2 \\
 & - \frac{\eta_1 \lambda_2}{\eta_2} \int_{\Omega} (u_2 - u_2^*)^2 - d_3 \delta_1 \int_{\Omega} |\nabla v_1|^2 + \Gamma_1 \frac{\eta_1}{\eta_2} \int_{\Omega} (u_2 - u_2^*)^2 + \frac{a_1^2 \delta_1^2 \eta_2}{4\Gamma_1 \eta_1} \int_{\Omega} (v_1 - v_1^*)^2 \\
 & - b_1 \delta_1 \int_{\Omega} (v_1 - v_1^*)^2 - d_4 \delta_2 \int_{\Omega} |\nabla v_2|^2 + \Gamma_2 \int_{\Omega} (u_1 - u_1^*)^2 + \frac{a_2^2 \delta_2^2}{4\Gamma_2} \int_{\Omega} (v_2 - v_2^*)^2 \\
 & - b_2 \delta_2 \int_{\Omega} (v_2 - v_2^*)^2 \\
 \leq & -(\lambda_1 - \Gamma_2) \int_{\Omega} (u_1 - u_1^*)^2 - \frac{\eta_1}{\eta_2} (\lambda_2 - \Gamma_1) \int_{\Omega} (u_2 - u_2^*)^2 \\
 & - \left( b_1 \delta_1 - \frac{a_1^2 \delta_1^2 \eta_2}{4\Gamma_1 \eta_1} \right) \int_{\Omega} (v_1 - v_1^*)^2 - \left( b_2 \delta_2 - \frac{a_2^2 \delta_2^2}{4\Gamma_2} \right) \int_{\Omega} (v_2 - v_2^*)^2 \\
 & - \left( d_3 \delta_1 - \frac{d_{12}^2 u_1^*}{4d_{11} \|u_1\|_{\mathcal{L}^\infty(\Omega)}^2} \right) \int_{\Omega} |\nabla v_1|^2 - \left( d_4 \delta_2 - \frac{d_{22}^2 \eta_1 u_2^*}{4d_{21} \eta_2 \|u_2\|_{\mathcal{L}^\infty(\Omega)}^2} \right) \int_{\Omega} |\nabla v_2|^2.
 \end{aligned}$$

Therefore, we get

$$\frac{d}{dt} \mathcal{E}_1(t) \leq -\epsilon_1 \left( \int_{\Omega} (u_1 - u_1^*)^2 + \int_{\Omega} (u_2 - u_2^*)^2 + \int_{\Omega} (v_1 - v_1^*)^2 + \int_{\Omega} (v_2 - v_2^*)^2 \right),$$

we arrive at (5.1) with  $\epsilon_1 > 0$ .  $\square$

**Lemma 5.4.** *Suppose  $(u_1^*, u_2^*, v_1^*, v_2^*)$  be the coexistence state of (2.1), then the following asymptotic behavior holds*

$$\|u_1(\cdot, t) - u_1^*\|_{\mathcal{L}^\infty(\Omega)} + \|u_2(\cdot, t) - u_2^*\|_{\mathcal{L}^\infty(\Omega)} + \|v_1(\cdot, t) - v_1^*\|_{\mathcal{L}^\infty(\Omega)} + \|v_2(\cdot, t) - v_2^*\|_{\mathcal{L}^\infty(\Omega)} \rightarrow 0 \quad (5.7)$$

as  $t \rightarrow \infty$ .

*Proof.* From (5.1), we have

$$\frac{d}{dt} \mathcal{E}_1(t) \leq -\epsilon_1 f_1(t), \quad t > 0.$$

Integrating over  $t$ , we get

$$\int_1^\infty f_1(t) \leq \frac{1}{\epsilon_1} (\mathcal{E}_1(1) - \mathcal{E}_1(t)) < \infty.$$

Lemma 5.1 implies that  $u_1$ ,  $u_2$ ,  $v_1$ , and  $v_2$  are uniformly Hölder continuous in  $\bar{\Omega} \times [t, t+1]$  with respect to  $t$ . Using Theorem 2.1, we establish that  $(u_1(\cdot, t))_{t>1}$  is bounded in  $\mathcal{W}^{1,\infty}(\Omega)$ . Therefore,  $f_1(t)$  is uniformly continuous in  $(1, \infty)$ , as stated in Lemma (5.2), which yields

$$\int_\Omega (u_1(\cdot, t) - u_1^*)^2 + \int_\Omega (u_2(\cdot, t) - u_2^*)^2 + \int_\Omega (v_1(\cdot, t) - v_1^*)^2 + \int_\Omega (v_2(\cdot, t) - v_2^*)^2 \rightarrow 0$$

as  $t \rightarrow \infty$ . Applying the Gagliardo-Nirenberg inequality, we have

$$\|u_1(\cdot, t) - u_1^*\|_{\mathcal{L}^\infty(\Omega)} \leq C_1 \|u_1(\cdot, t) - u_1^*\|_{\mathcal{W}^{1,\infty}(\Omega)}^{\frac{n}{n+2}} \|u_1(\cdot, t) - u_1^*\|_{\mathcal{L}^2(\Omega)}^{\frac{2}{n+2}}, \quad t > 0. \quad (5.8)$$

As a consequence, we can infer that  $u_1(\cdot, t)$  converges to  $u_1^*$  in  $\mathcal{L}^\infty(\Omega)$  when  $t$  tends to infinity. Similarly, through analogous reasoning, we can obtain (5.7).  $\square$

**5.2. Prey vanishing state.** Here we assume that  $\eta_2 \geq \frac{\mu_2 \lambda_1}{\mu_1}$  and

$$d_{12}^2 < \frac{16d_{11}d_3b_1\eta_1\lambda_1\lambda_2\|u_1\|_{\mathcal{L}^\infty(\Omega)}^2}{a_1^2\mu_1\eta_2}$$

hold. Let  $(u_1, u_2, v_1, v_2)$  be the classical solution of (2.1) satisfying (2.3). The proof is similar to the previous Lemmas 5.3 and 5.4.

**Lemma 5.5.** *There exists  $\delta_2, \delta_3 > 0$  and  $\epsilon_2 > 0$  such that the functions*

$$\mathcal{E}_2(t) = \int_\Omega \left( u_1 - \frac{\mu_1}{\lambda_1} - \frac{\mu_1}{\lambda_1} \ln \frac{u_1}{\mu_1} \right) + \frac{\eta_1}{\eta_2} \int_\Omega u_2 + \frac{\delta_3}{2} \int_\Omega v_1^2 + \frac{\delta_4}{2} \int_\Omega \left( v_2 - \frac{\mu_1 a_2}{\lambda_1 b_2} \right)^2$$

and

$$f_2(t) = \int_\Omega \left( u_1 - \frac{\mu_1}{\lambda_1} \right)^2 + \int_\Omega u_2^2 + \int_\Omega v_1^2 + \int_\Omega \left( v_2 - \frac{\mu_1 a_2}{\lambda_1 b_2} \right)^2$$

satisfy

$$\frac{d}{dt} \mathcal{E}_2(t) \leq -\epsilon_2 f_2(t) - \left( \frac{\eta_1 \mu_1}{\lambda_1} - \frac{\eta_1 \mu_2}{\eta_2} \right) \int_\Omega u_2, \quad t > 0, \quad (5.9)$$

where  $\epsilon_2 > 0$ .

*Proof.* Choose  $\eta_3 \in (0, \delta_3 b_1)$  and  $\eta_4 \in (0, \lambda_1)$  and fix  $\delta_3 \in \left( \frac{d_{12}^2 \mu_1}{4d_{11}d_3\lambda_1 \|u_1\|_{\mathcal{L}^\infty(\Omega)}^2}, \frac{4b_1\eta_1\lambda_2}{a_1^2\eta_2} \right)$  and  $\delta_4 \in \left( 0, \frac{4b_2\lambda_1}{a_2^2} \right)$ . Consider the energy functional as follows

$$\mathcal{E}_2(t) = \mathcal{A}_2(t) + \frac{\eta_1}{\eta_2} \mathcal{B}_2(t) + \mathcal{C}_2(t) + \mathcal{D}_2(t), \quad t > 0,$$

A simple computation gives

$$\begin{aligned} \frac{d}{dt} \mathcal{A}_2(t) &= -\frac{d_{11}\mu_1}{\lambda_1} \int_{\Omega} \left| \frac{\nabla u_1}{u_1} \right|^2 - \frac{d_{12}\mu_1}{\lambda_1} \int_{\Omega} \frac{\nabla u_1}{u_1^2} \cdot \nabla v_1 + \frac{1}{\lambda_1} \int_{\Omega} (\lambda_1 u_1 - \mu_1)(\mu_1 - \lambda_1 u_1 + \eta_1 u_2) \\ &= \frac{d_{12}^2 \mu_1}{4d_{11}\lambda_1 \|u_1\|_{\mathcal{L}^\infty(\Omega)}^2} \int_{\Omega} |\nabla v_1|^2 + \frac{1}{\lambda_1} \int_{\Omega} (\lambda_1 u_1 - \mu_1)(\mu_1 - \lambda_1 u_1 + \eta_1 u_2) \end{aligned}$$

and

$$\frac{d}{dt} \mathcal{B}_2(t) = \int_{\Omega} u_2(\mu_2 - \lambda_2 u_2 - \eta_2 u_1).$$

Similarly, we get

$$\frac{d}{dt} \mathcal{C}_2(t) = -d_3 \delta_3 \int_{\Omega} |\nabla v_1|^2 + a_1 \delta_3 \int_{\Omega} v_1 u_2 - \delta_3 b_1 \int_{\Omega} v_1^2.$$

Employing Cauchy's inequality, the second expression on the right-hand side of the previous estimation yields

$$\frac{d}{dt} \mathcal{C}_2(t) \leq -d_3 \delta_3 \int_{\Omega} |\nabla v_1|^2 + \eta_3 \int_{\Omega} v_1^2 + \frac{a_1^2 \delta_3^2}{4\eta_3} \int_{\Omega} u_2^2 - \delta_3 b_1 \int_{\Omega} v_1^2.$$

By a similar fashion, we obtain

$$\begin{aligned} \frac{d}{dt} \mathcal{D}_2(t) &= -d_4 \delta_4 \int_{\Omega} |\nabla v_2|^2 + a_2 \delta_4 \int_{\Omega} \left( v_2 - \frac{\mu_1 a_2}{\lambda_1 b_2} \right) u_1 - b_2 \delta_4 \int_{\Omega} \left( v_2 - \frac{\mu_1 a_2}{\lambda_1 b_2} \right) v_2 \\ &= -d_4 \delta_4 \int_{\Omega} |\nabla v_2|^2 + a_2 \delta_4 \int_{\Omega} \left( v_2 - \frac{\mu_1 a_2}{\lambda_1 b_2} \right) u_1 - b_2 \delta_4 \int_{\Omega} \left( v_2 - \frac{\mu_1 a_2}{\lambda_1 b_2} \right) v_2 \\ &\quad + b_2 \delta_4 \int_{\Omega} \left( v_2 - \frac{\mu_1 a_2}{\lambda_1 b_2} \right) \frac{\mu_1 a_2}{\lambda_1 b_2} - b_2 \delta_4 \int_{\Omega} \left( v_2 - \frac{\mu_1 a_2}{\lambda_1 b_2} \right) \frac{\mu_1 a_2}{\lambda_1 b_2} \\ &= -d_4 \delta_4 \int_{\Omega} |\nabla v_2|^2 + a_2 \delta_4 \int_{\Omega} \left( v_2 - \frac{\mu_1 a_2}{\lambda_1 b_2} \right) \left( u_1 - \frac{\mu_1}{\lambda_1} \right) - b_2 \delta_4 \int_{\Omega} \left( v_2 - \frac{\mu_1 a_2}{\lambda_1 b_2} \right)^2. \end{aligned}$$

By making use of Cauchy's inequality, the second term on the right-hand side of the aforementioned estimation yields

$$\begin{aligned} \frac{d}{dt} \mathcal{D}_2(t) &\leq -d_4 \delta_4 \int_{\Omega} |\nabla v_2|^2 + \eta_4 \int_{\Omega} \left( u_1 - \frac{\mu_1}{\lambda_1} \right)^2 + \frac{a_2^2 \delta_4^2}{4\eta_4} \int_{\Omega} \left( v_2 - \frac{\mu_1 a_2}{\lambda_1 b_2} \right)^2 \\ &\quad - b_2 \delta_4 \int_{\Omega} \left( v_2 - \frac{\mu_1 a_2}{\lambda_1 b_2} \right)^2. \end{aligned}$$

By consolidating all the terms, it is possible to derive

$$\begin{aligned} \frac{d}{dt} \mathcal{E}_2(t) &\leq -\left( \frac{\eta_1 \mu_1}{\lambda_1} - \frac{\eta_1 \mu_2}{\eta_2} \right) \int_{\Omega} u_2 - (\lambda_1 - \eta_4) \int_{\Omega} \left( u_1 - \frac{\mu_1}{\lambda_1} \right)^2 - \left( \frac{\eta_1 \lambda_2}{\eta_2} - \frac{a_1^2 \delta_3^2}{4\eta_3} \right) \int_{\Omega} u_2^2 \\ &\quad - (\delta_3 b_1 - \eta_3) \int_{\Omega} v_1^2 - \left( b_2 \delta_4 - \frac{a_2^2 \delta_4^2}{4\eta_4} \right) \int_{\Omega} \left( v_2 - \frac{\mu_1 a_2}{\lambda_1 b_2} \right)^2 \end{aligned}$$

$$- \left( d_3 \delta_3 - \frac{d_{12}^2 \mu_1}{4d_{11} \lambda_1 \|u_1\|_{\mathcal{L}^\infty(\Omega)}^2} \right) \int_{\Omega} |\nabla v_1|^2 - d_4 \delta_4 \int_{\Omega} |\nabla v_2|^2,$$

which implies (5.9) with  $\epsilon_2 > 0$ .  $\square$

**Lemma 5.6.** *Suppose  $\left(\frac{\mu_1}{\lambda_1}, 0, 0, \frac{\mu_1 a_2}{\lambda_1 b_2}\right)$  be the positive semi-trivial equilibrium of (2.1), then the following asymptotic behavior holds*

$$\left\| u_1(\cdot, t) - \frac{\mu_1}{\lambda_1} \right\|_{\mathcal{L}^\infty(\Omega)} + \left\| u_2(\cdot, t) \right\|_{\mathcal{L}^\infty(\Omega)} + \left\| v_1(\cdot, t) \right\|_{\mathcal{L}^\infty(\Omega)} + \left\| v_2(\cdot, t) - \frac{\mu_1 a_2}{\lambda_1 b_2} \right\|_{\mathcal{L}^\infty(\Omega)} \rightarrow 0$$

as  $t \rightarrow \infty$ .

*Proof.* In view of Lemma 5.4, the proof is similar.  $\square$

We demonstrate the subsequent theorems using Lemmas 5.4, 5.6, which possess uniform convergence properties.

**Proof of Theorem 2.2.** Now, let  $\mathcal{H}(u) = u - u_1(\cdot, s) \ln u$ , for  $u > 0$ , from L'Hôspital's rule, we have

$$\lim_{u_1 \rightarrow u_1^*} \frac{\mathcal{H}(u_1) - \mathcal{H}(u_1^*)}{(u_1 - u_1^*)^2} = \frac{1 - \frac{u_1^*}{u_1}}{2(u_1 - u_1^*)} = \frac{1}{2u_1^*}.$$

We can thus choose  $t_0 > 0$  and by the Taylor's expansion such that

$$\int_{\Omega} \left( u_1 - u_1^* - u_1^* \ln \frac{u_1}{u_1^*} \right) = \int_{\Omega} (\mathcal{H}(u_1) - \mathcal{H}(u_1^*)) \leq \frac{1}{2u_1^*} \int_{\Omega} (u_1 - u_1^*)^2, \quad \forall t > t_0.$$

From the above estimate, we arrive at

$$\frac{1}{4u_1^*} \int_{\Omega} (u_1 - u_1^*)^2 \leq \int_{\Omega} \left( u_1 - u_1^* - u_1^* \ln \frac{u_1}{u_1^*} \right) \leq \frac{3}{4u_1^*} \int_{\Omega} (u_1 - u_1^*)^2, \quad \forall t > t_0. \quad (5.10)$$

Similarly, we can arrive at

$$\frac{1}{4u_2^*} \int_{\Omega} (u_2 - u_2^*)^2 \leq \int_{\Omega} \left( u_2 - u_2^* - u_2^* \ln \frac{u_2}{u_2^*} \right) \leq \frac{3}{4u_2^*} \int_{\Omega} (u_2 - u_2^*)^2, \quad \forall t > t_0. \quad (5.11)$$

Considering the right-hand sides of the inequalities (5.10) and (5.11), it becomes apparent that for all  $t > t_0$  and with  $C_1 > 0$ ,  $\mathcal{E}_1(t) \leq C_1 \mathcal{F}_1(t)$ . This result is supported by Lemma 5.3, which states that

$$\frac{d}{dt} \mathcal{E}_1(t) \leq -\epsilon_1 f_1(t) \leq -\frac{\epsilon_1}{C_1} \mathcal{E}_1(t), \quad t > t_0.$$

Solving the above differential inequality, gives

$$\mathcal{E}_1(t) \leq C_2 e^{-\frac{\epsilon_1}{C_1} t}, \quad t > t_0.$$

By utilizing the solution provided earlier, we can derive expressions from the left-hand side of the inequalities (5.10) and (5.11), resulting in the following

$$f_1(t) \leq C_3 \mathcal{E}_1(t) \leq C_4 e^{-\frac{\epsilon_1}{C_1} t}, \quad t > t_0.$$

Using (5.8) and Lemma 5.1, finally we arrive at

$$\begin{aligned} \left\| u_1(\cdot, t) - u_1^* \right\|_{\mathcal{L}^\infty(\Omega)} + \left\| u_2(\cdot, t) - u_2^* \right\|_{\mathcal{L}^\infty(\Omega)} + \left\| v_1(\cdot, t) - v_1^* \right\|_{\mathcal{L}^\infty(\Omega)} \\ + \left\| v_2(\cdot, t) - v_2^* \right\|_{\mathcal{L}^\infty(\Omega)} \leq C_6 e^{-\frac{\epsilon_1}{C_1} t}, \end{aligned}$$

for all  $t > t_0$ .  $\square$

**Proof of Theorem 2.3.** Assuming  $\eta_2 > \frac{\mu_2 \lambda_1}{\mu_1}$  and choose  $t_0 > 0$ , we can use a comparable approach to that used to derive (5.10) and (5.11) to arrive at the following result

$$\frac{\lambda_1}{4\mu_1} \int_{\Omega} \left( u_1 - \frac{\mu_1}{\lambda_1} \right)^2 \leq \int_{\Omega} \left( u_1 - \frac{\mu_1}{\lambda_1} - \frac{\mu_1}{\lambda_1} \ln \frac{u_1}{\mu_1} \right) \leq \frac{3\lambda_1}{4\mu_1} \int_{\Omega} \left( u_1 - \frac{\mu_1}{\lambda_1} \right)^2, \quad \forall t > t_0. \quad (5.12)$$

and

$$\frac{1}{2} \int_{\Omega} u_2^2 + \frac{1}{2} \int_{\Omega} u_2 \leq \int_{\Omega} u_2 \leq 2 \int_{\Omega} u_2^2 + 2 \int_{\Omega} u_2, \quad \forall t > t_0. \quad (5.13)$$

Considering the right-hand side of inequalities (5.12) and (5.13), it is apparent that  $\mathcal{E}_2(t) \leq C_7 (f_2(t) + \int_{\Omega} u_2)$  for all  $t > t_0$  with  $C_7 > 0$ . In light of Lemma 5.5, with  $\left( \frac{\eta_1 \mu_1}{\lambda_1} - \frac{\eta_1 \mu_2}{\eta_2} \right) > \epsilon_2$ , we obtain

$$\frac{d}{dt} \mathcal{E}_2(t) \leq -\frac{\epsilon_2}{C_7} \mathcal{E}_2(t) - \left( \left( \frac{\eta_1 \mu_1}{\lambda_1} - \frac{\eta_1 \mu_2}{\eta_2} \right) - \epsilon_2 \right) \int_{\Omega} u_2 \leq -\frac{\epsilon_2}{C_7} \mathcal{E}_2(t), \quad t > t_0,$$

such that  $\mathcal{E}_2(t) \leq C_8 e^{-\frac{\epsilon_2}{C_7} t}$ ,  $t > t_0$ . Examining the left-hand side of inequalities (5.12) and (5.13), we can see that  $f_2(t) \leq C_9 \mathcal{E}_2(t) \leq C_{10} e^{-\frac{\epsilon_2}{C_7} t}$ . Hence we get

$$\left\| u_1(\cdot, t) - \mu_1 \right\|_{\mathcal{L}^{\infty}(\Omega)} + \left\| u_2(\cdot, t) \right\|_{\mathcal{L}^{\infty}(\Omega)} + \left\| v_1(\cdot, t) \right\|_{\mathcal{L}^{\infty}(\Omega)} + \left\| v_2(\cdot, t) - \frac{\mu_1 a_2}{\lambda_1 b_2} \right\|_{\mathcal{L}^{\infty}(\Omega)} \leq C_{12} e^{-\frac{\epsilon_2}{C_7} t}.$$

for all  $t > t_0$ .

In addition, in the case where  $\eta_2 = \frac{\mu_2 \lambda_1}{\mu_1}$ , we find that  $\left( \frac{\eta_1 \mu_1}{\lambda_1} - \frac{\eta_1 \mu_2}{\eta_2} \right) \int_{\Omega} u_2 = 0$ . Nevertheless, it is worth noting that (5.12) and (5.13) still remain valid. By utilizing the inequality on the right-hand side of (5.12) and applying Cauchy-Schwarz inequality with  $C_{13}, C_{14} > 0$ , we obtain

$$\begin{aligned} \mathcal{E}_2(t) &\leq C_{13} \int_{\Omega} \left( u_1 - \frac{\mu_1}{\lambda_1} \right)^2 + C_{13} \int_{\Omega} u_2 + C_{13} \int_{\Omega} v_1^2 + C_{13} \int_{\Omega} \left( v_2 - \frac{\mu_1 a_2}{\lambda_1 b_2} \right)^2 \\ &\leq C_{14} \left( \int_{\Omega} \left( u_1 - \frac{\mu_1}{\lambda_1} \right)^2 \right)^{\frac{1}{2}} + C_{14} \left( \int_{\Omega} u_2^2 \right)^{\frac{1}{2}} + C_{14} \left( \int_{\Omega} v_1^2 \right)^{\frac{1}{2}} + C_{14} \left( \int_{\Omega} \left( v_2 - \frac{\mu_1 a_2}{\lambda_1 b_2} \right)^2 \right)^{\frac{1}{2}} \\ &\leq C_{15} f_2^{\frac{1}{2}}(t), \quad \forall t > t_0, \end{aligned}$$

such that

$$\frac{d}{dt} \mathcal{E}_2(t) \leq -\epsilon_2 f_2(t) \leq -\frac{\epsilon_2}{C_{16}} \mathcal{E}_2^2(t), \quad t > t_0.$$

Hence, we obtain the solution of the above ODE problem as  $\mathcal{E}_2(t) \leq \frac{C_{18}}{\epsilon_2 t + C_{17}}$ . From the left hand side inequalities (5.12) and (5.13), we have

$$\int_{\Omega} \left( u_1 - \frac{\mu_1}{\lambda_1} \right)^2 + \int_{\Omega} u_2^2 + \int_{\Omega} v_1^2 + \int_{\Omega} \left( v_2 - \frac{\mu_1 a_2}{\lambda_1 b_2} \right)^2 \leq C_{19} \mathcal{E}_2(t) \leq \frac{C_{20}}{\epsilon_2 t + C_{17}}.$$

Finally, we obtain

$$\left\| u_1(\cdot, t) - \frac{\mu_1}{\lambda_1} \right\|_{\mathcal{L}^{\infty}(\Omega)} + \left\| u_2(\cdot, t) \right\|_{\mathcal{L}^{\infty}(\Omega)} + \left\| v_1(\cdot, t) \right\|_{\mathcal{L}^{\infty}(\Omega)} + \left\| v_2(\cdot, t) - \frac{\mu_1 a_2}{\lambda_1 b_2} \right\|_{\mathcal{L}^{\infty}(\Omega)} \leq \frac{C_{22}}{\epsilon_2 t + C_{17}},$$

for all  $t > t_0$ , hence complete the proof.  $\square$

**Remark 5.1.** *It is not generally possible to achieve exponential convergence by assuming  $\eta_2 = \frac{\mu_2 \lambda_1}{\mu_1}$  in (5.9).*

## 6. BIFURCATION ANALYSIS

We investigate the cross-diffusion-driven instability of the spatially homogeneous steady state through a standard linear analysis. Turing instability occurs when a steady state that is locally stable in the absence of diffusion becomes unstable under spatially non-uniform perturbations due to the presence of cross-diffusion. We begin by analyzing the local stability of system (2.1) without the diffusion terms. The non-diffusive system can be written in the following form

$$\begin{cases} \frac{du_1}{dt} = u_1(\mu_1 - \lambda_1 u_1 + \eta_1 u_2), \\ \frac{du_2}{dt} = u_2(\mu_2 - \lambda_2 u_2 - \eta_2 u_1), \\ \frac{dv_1}{dt} = a_1 u_2 - b_1 v_1, \\ \frac{dv_2}{dt} = a_2 u_1 - b_2 v_2, \end{cases} \quad (6.1)$$

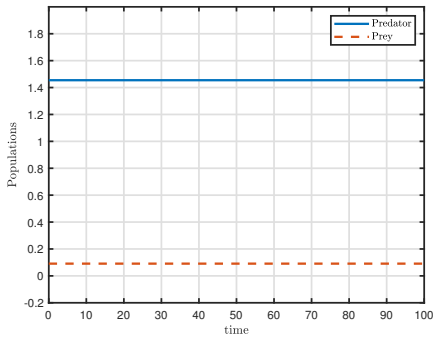
Then the Jacobian matrix for coexistence steady state is given by

$$J = \begin{pmatrix} \mu_1 - 2\lambda_1 u_1^* + \eta_1 u_2^* & \eta_1 u_1^* & 0 & 0 \\ -\eta_2 u_2^* & \mu_2 - 2\lambda_2 u_2^* - \eta_2 u_1^* & 0 & 0 \\ 0 & a_1 & -b_1 & 0 \\ a_2 & 0 & 0 & -b_2 \end{pmatrix}. \quad (6.2)$$

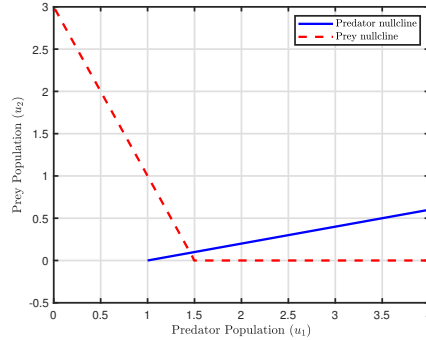
Thus, we get

$$J = \begin{pmatrix} -\lambda_1 u_1^* & \eta_1 u_1^* & 0 & 0 \\ -\eta_2 u_2^* & -\lambda_2 u_2^* & 0 & 0 \\ 0 & a_1 & -b_1 & 0 \\ a_2 & 0 & 0 & -b_2 \end{pmatrix} := \begin{pmatrix} J_{11} & J_{12} & 0 & 0 \\ J_{21} & J_{22} & 0 & 0 \\ 0 & a_1 & -b_1 & 0 \\ a_2 & 0 & 0 & -\beta \end{pmatrix}.$$

Here we use  $\mu_1 - \lambda_1 u_1^* + \eta_1 u_2^* = 0$  and  $\mu_2 - \lambda_2 u_2^* - \eta_2 u_1^* = 0$ . Then  $\text{Tr}(J) = -\lambda_1 u_1^* - \lambda_2 u_2^* - b_1 - b_2 < 0$  and  $\text{Det}(J) = \lambda_1 \lambda_2 u_1^* u_2^* b_1 b_2 + \eta_1 \eta_2 u_1^* u_2^* b_1 b_2 > 0$ . Therefore, the coexistence steady state  $(u_1^*, u_2^*, v_1^*, v_2^*)$  is locally asymptotically stable (LAS).



(A) LAS of the ODE system



(B) The nullclines of predator and prey

FIGURE 1. Parameters  $\mu_1 = 2, \mu_2 = 3, \lambda_1 = 2, \lambda_2 = 1, a_1 = a_2 = b_1 = b_2 = 0.5, \eta_1 = 10, \eta_2 = 2$ .

Turing patterns arise when diffusion destabilizes a spatially homogeneous steady state, leading to the spontaneous formation of stationary structures such as spots, stripes, or patches. In reaction-diffusion systems, this diffusion-driven instability amplifies specific spatial modes, producing ordered patterns without external forcing. In predator-prey models, Turing patterns

explain how spatial segregation or aggregation can emerge purely from species interactions. Cross-diffusion further enhances this mechanism by widening the instability regime and enabling richer, biologically realistic pattern formation [14].

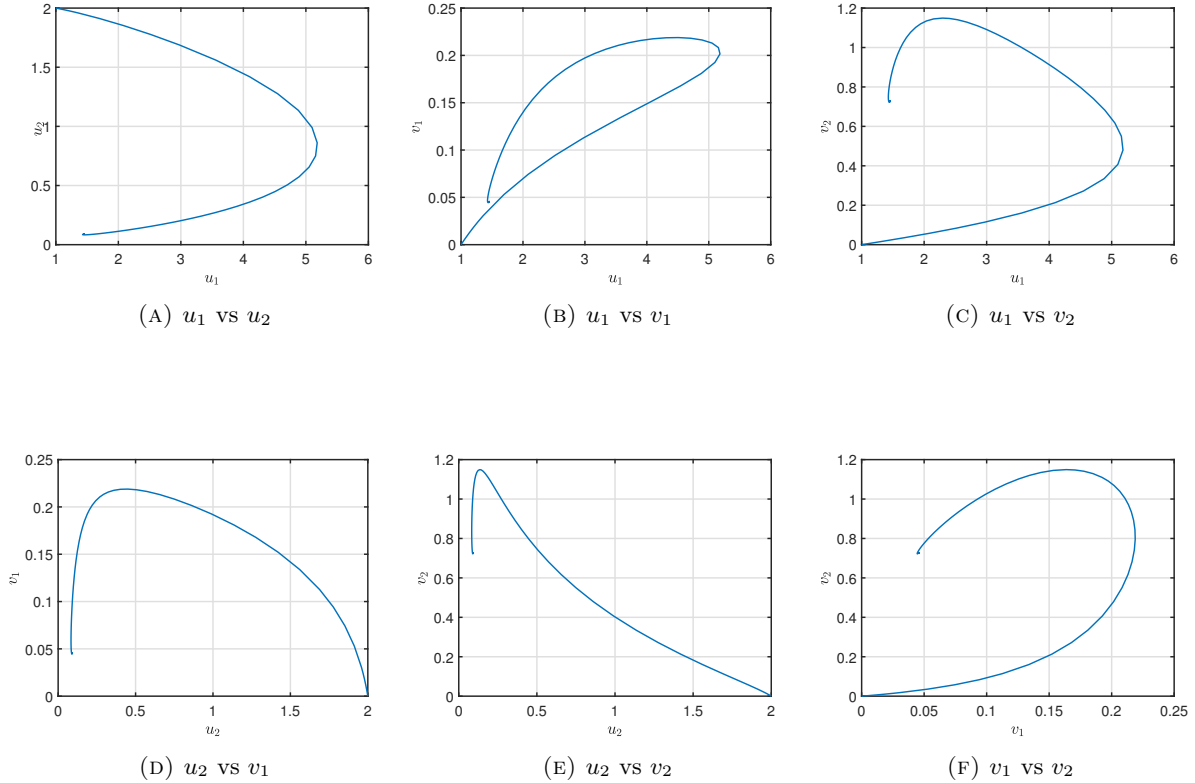


FIGURE 2. Phase portrait of the species and chemicals. Parameter values  $\mu_1 = 2, \mu_2 = 3, \lambda_1 = 2, \lambda_2 = 1, a_1 = a_2 = 1, b_1 = b_2 = 2, \eta_1 = 10, \eta_2 = 2$ . The initial condition is  $u_{10} = 1, u_{20} = 2, v_{10} = v_{20} = 0$ .

The above figure presents the phase portraits of the predator–prey system and their associated chemical signals for the given parameter set, where the trajectories represent the temporal evolution of the interacting biological populations and their chemical mediators. The  $u_1$ – $u_2$  plot illustrates the nonlinear interaction between predator and prey populations, indicating bounded coexistence dynamics. The portraits  $u_1$ – $v_1$  and  $u_2$ – $v_1$  describe the dependence of the prey-released chemical on prey density and its indirect influence on the predator population. Similarly,  $u_1$ – $v_2$  and  $u_2$ – $v_2$  show the relationship between predator density and the predator-associated chemical signal. The  $v_1$ – $v_2$  phase plot reflects the indirect coupling between the two chemical mediators through the predator–prey dynamics.

We now analyze the local stability of the system (2.1) with self-diffusion and assume that (2.2) hold. We consider small perturbations around the equilibrium

$$u(x, t) = u^* + w(x, t),$$

where  $w = (u_1, u_2, v_1, v_2)^T$ . Substituting into the system and linearizing, we obtain

$$w_t = d\Delta w + Jw,$$

where,  $d$  is the diffusion matrix,  $J$  is the Jacobian evaluated at  $u^*$ . We assume perturbations are of the form

$$w(x, t) = ce^{\lambda t + ik \cdot x},$$

where  $k$  is the wave vector (spatial frequency),  $c$  is the time-dependent amplitude of the mode,  $e^{\lambda t + ik \cdot x}$  is the sinusoidal spatial variation and  $\lambda$  is the growth rate. Substituting, we get

$$\lambda ce^{\lambda t + ik \cdot x} = -k^2 d ce^{\lambda t + ik \cdot x} + J ce^{\lambda t + ik \cdot x}.$$

The dispersion relation is given by  $\text{Det}(-k^2 d + J - \lambda I) = 0$ . That is

$$\begin{vmatrix} -k^2 d_{11} - \lambda_1 u_1^* - \lambda & \eta_1 u_1^* \\ -\eta_2 u_2^* & -k^2 d_{21} - \lambda_2 u_2^* - \lambda \end{vmatrix} = 0.$$

We can easily check  $\text{Trace} = -k^2 d_{11} - \lambda_1 u_1^* - k^2 d_{21} - \lambda_2 u_2^* < 0$  and  $\text{Det} = (k^2 d_{11} + \lambda_1 u_1^*)(k^2 d_{21} + \lambda_2 u_2^*) + \eta_1 \eta_2 u_1^* u_2^* > 0$ .

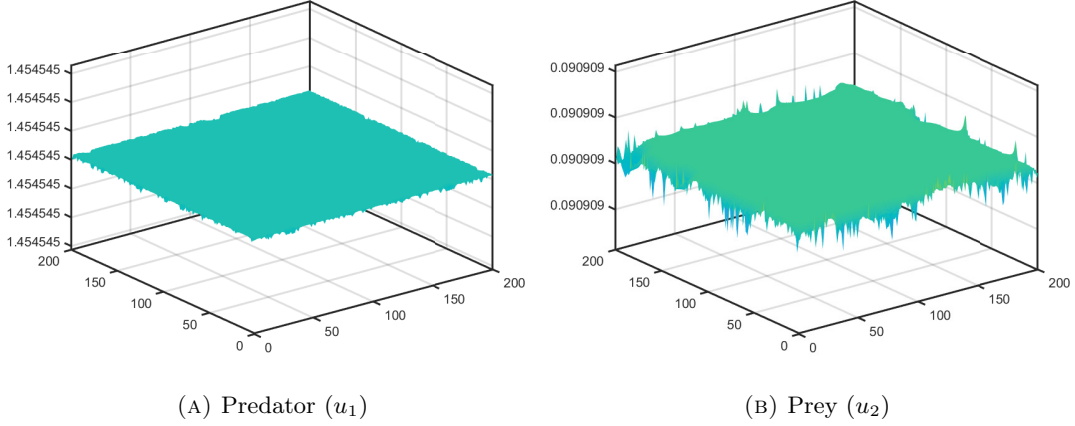


FIGURE 3. LAS of the coexistence state of system (2.1) for the parameter values  $d_{11} = 0.1, d_{12} = 0, d_3 = 3, d_{21} = 1, d_{22} = 0, d_4 = 2, \mu_1 = 2, \mu_2 = 3, \lambda_1 = 2, \lambda_2 = 1, a_1 = a_2 = b_1 = b_2 = 0.5, \eta_1 = 10, \eta_2 = 2$  and  $t = 1000$ .

Therefore, the coexistence steady state  $(u_1^*, u_2^*, v_1^*, v_2^*)$  is locally asymptotically stable. Moreover, both the corresponding ODE system and the reaction–diffusion system incorporating self-diffusion remain locally asymptotically stable around this equilibrium point. Our analysis indicates that self-diffusion alone is insufficient to induce spatial pattern formation. Consequently, to explore the emergence of spatial patterns, we extend the model by incorporating cross-diffusion effects into the system. For the cross-diffusion system, we have

$$\begin{vmatrix} -k^2 d_{11} + J_{11} - \lambda & J_{12} & -k^2 d_{12} & 0 \\ J_{21} & -k^2 d_{21} + J_{22} - \lambda & 0 & k^2 d_{22} \\ 0 & a_1 & -k^2 d_3 - b_1 - \lambda & 0 \\ a_2 & 0 & 0 & -k^2 d_4 - b_2 - \lambda \end{vmatrix} = 0.$$

General form of the characteristic polynomial is

$$\lambda^4 + A_1 \lambda^3 + A_2 \lambda^2 + A_3 \lambda + A_4 = 0. \quad (6.3)$$

Sufficient condition for cross-diffusion driven instability is  $A_4 < 0$ , where

$$\begin{aligned}
 A_4 = & k^8 d_3 d_4 d_{11} d_{21} + k^6 \left( \lambda_1 d_3 d_4 d_{21} u_1 + \lambda_2 d_3 d_4 d_{11} u_2 + b_1 d_4 d_{11} d_{21} + b_2 d_3 d_{11} d_{21} \right) \\
 & + k^4 \left( \lambda_2 b_1 d_4 d_{11} u_2 + \lambda_2 b_2 d_3 d_{11} u_2 + \lambda_1 b_1 d_4 d_{21} u_1 + \lambda_1 b_2 d_3 d_{21} u_1 + \lambda_1 \lambda_2 d_3 d_4 u_1 u_2 \right. \\
 & \quad \left. + \alpha_1 \alpha_2 d_{12} d_{22} + b_1 b_2 d_{11} d_{21} + d_3 d_4 \eta_1 \eta_2 u_1 u_2 - a_1 d_4 d_{12} \eta_2 u_2 - a_2 d_3 d_{22} \eta_1 u_1 \right) \\
 & + k^2 \left( \lambda_1 \lambda_2 b_1 d_4 u_1 u_2 + \lambda_1 b_2 b_1 d_{21} u_1 + \lambda_2 b_2 b_1 d_{11} u_2 + \lambda_1 \lambda_2 b_2 d_3 u_1 u_2 + b_1 d_4 \eta_1 \eta_2 u_1 u_2 \right. \\
 & \quad \left. + b_2 d_3 \eta_1 \eta_2 u_1 u_2 - a_2 b_1 d_{22} \eta_1 u_1 - a_1 b_2 d_{12} \eta_2 u_2 \right) \\
 & + \lambda_1 \lambda_2 b_1 b_2 u_1 u_2 + b_1 b_2 \eta_1 \eta_2 u_1 u_2
 \end{aligned}$$

This can be written as  $h(k^2) = \omega_1 k^4 + \omega_2 k^3 + \omega_3 k^2 + \omega_4 k + \omega_5$ , where we assume  $\omega_i > 0, i = 1, 2, \dots, 5$ . Clearly,  $\omega_5 > 0$ , this means the polynomial evaluated at  $k^2 = 0$  is positive. The roots are given by

$$\begin{aligned}
 k_{1,2}^2 = & -\frac{\omega_2}{4\omega_1} - \frac{1}{2}\beta_4 \pm \frac{1}{2} \sqrt{\frac{\omega_2^2}{2\omega_1^2} - \frac{4\omega_3}{3\omega_1} - \frac{2^{\frac{1}{3}}\beta_1}{3\omega_1\beta_3^{\frac{1}{3}}} - \frac{\beta_3^{\frac{1}{3}}}{3 \times 2^{\frac{1}{3}}\omega_1} + \frac{\frac{\omega_2^3}{\omega_1^3} - \frac{4\omega_3\omega_2}{\omega_1^2} + \frac{8\omega_4}{\omega_1}}{4\beta_4}}, \\
 k_{3,4}^2 = & -\frac{\omega_2}{4\omega_1} + \frac{1}{2}\beta_4 \pm \frac{1}{2} \sqrt{\frac{\omega_2^2}{2\omega_1^2} - \frac{4\omega_3}{3\omega_1} - \frac{2^{\frac{1}{3}}\beta_1}{3\omega_1\beta_3^{\frac{1}{3}}} - \frac{\beta_3^{\frac{1}{3}}}{3 \times 2^{\frac{1}{3}}\omega_1} + \frac{\frac{\omega_2^3}{\omega_1^3} - \frac{4\omega_3\omega_2}{\omega_1^2} + \frac{8\omega_4}{\omega_1}}{4\beta_4}},
 \end{aligned}$$

where

$$\begin{aligned}
 \beta_1 = & \omega_3^2 - 3\omega_2\omega_4 + 12\omega_1\omega_5, & \beta_2 = & 2\omega_3^3 - 9\omega_2\omega_4\omega_3 - 72\omega_1\omega_5\omega_3 + 27\omega_1\omega_4^2 + 27\omega_2^2\omega_5, \\
 \beta_3 = & \beta_2 + \sqrt{-4\beta_1^3 + \beta_2^2}, & \beta_4 = & \sqrt{\frac{\omega_2^2}{4\omega_1^2} - \frac{2\omega_3}{3\omega_1} + \frac{2^{\frac{1}{3}}\beta_1}{3\omega_1\beta_3^{\frac{1}{3}}} + \frac{\beta_3^{\frac{1}{3}}}{3 \times 2^{\frac{1}{3}}\omega_1}}.
 \end{aligned}$$

In general, deriving explicit analytical conditions for the onset of a Turing bifurcation is highly challenging due to the complexity of the associated characteristic equations. Consequently, we rely on numerical simulations to identify the emergence of Turing patterns and to determine the corresponding admissible values of  $k^2$ .

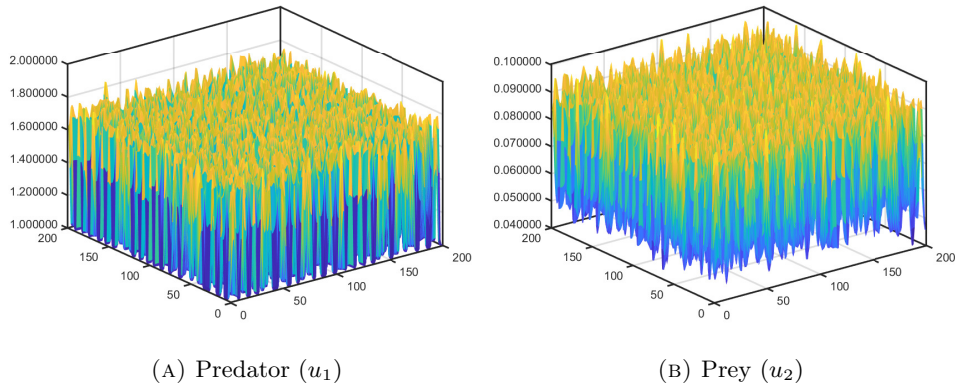


FIGURE 4. Cross-diffusion driven instability of the system (2.1) for the parameter values  $d_{11} = 0.1, d_{12} = 1, d_3 = 3, d_{21} = 1, d_{22} = 2, d_4 = 2, \mu_1 = 2, \mu_2 = 3, \lambda_1 = 2, \lambda_2 = 1, a_1 = a_2 = b_1 = b_2 = 0.5, \eta_1 = 10, \eta_2 = 2$  and  $t = 1000$ .

We now introduce the finite difference method to conduct numerical simulations and investigate the temporal and spatial dynamics of the predator–prey system (2.1). We consider the square domain  $[0, 200]^2$  with a maximum simulation time of  $T_{\max} = 5000$ . To implement our iterative scheme, we choose spatial steps  $\Delta x = \Delta y = 1$  and a time step  $\Delta t = 0.01$ . In addition, the initial population distributions are taken as small-amplitude random perturbations around the coexistence steady state  $(u_1^*, u_2^*, v_1^*, v_2^*)$  as

$$\begin{aligned} u_1(\cdot, 0) &= u_1^* - 2 \times 10^{-4} \psi & \text{and} & & u_2(\cdot, 0) &= u_2^* + 2 \times 10^{-4} \psi, \\ v_1(\cdot, 0) &= v_1^* + 2 \times 10^{-4} \psi & \text{and} & & v_2(\cdot, 0) &= v_2^* - 2 \times 10^{-4} \psi, \end{aligned}$$

where  $\psi$  is a random-number matrix whose entries lie between 0 and 200. Using the parameter sets employed in Figures 6 - 11, we determine the positive ranges of  $k^2$  that give rise to diffusion-driven instability, as summarized in the following table.

TABLE 1. Turing bifurcation is observed for  $k^2$  in Figures 6 - 11.

Figure	Parameter values	range of $k^2$
6	$\eta_2 = 2$	[0.253661, 0.925807]
	$\eta_2 = 2.25$	[0.138333, 1.255916]
	$\eta_2 = 2.5$	[0.074781, 1.526103]
7	$\eta_2 = 2.65$	[0.047290, 1.673559]
	$\eta_2 = 2.75$	[0.031782, 1.767353]
	$\eta_2 = 2.9$	[0.011695, 1.902321]
8	$\eta_1 = 5, \eta_2 = 0.95$	[0.026322, 0.092956]
	$\eta_1 = 10, \eta_2 = 0.25$	[0.100961, 0.512843]
	$\eta_1 = 10, \eta_2 = 0.75$	[0.027417, 0.442167]
9	$\eta_1 = 5, \eta_2 = 0.075$	[0.001004, 0.433782]
	$\eta_1 = 10, \eta_2 = 0.075$	[0.000455, 0.803716]
10	$\eta_1 = 10, \eta_2 = 1$	[0.185205, 0.581330]
	$\eta_1 = 10, \eta_2 = 1.5$	[0.110821, 0.675433]
11	(a)	[1.102053, 12.303332]
	(b)	[0.485184, 5.105713]

Interestingly, predator ( $u_1$ ) and prey ( $u_2$ ) often exhibit maxima and minima at the same spatial locations because their movements are strongly regulated by the prey chemical ( $v_1$ ) and predator chemical ( $v_2$ ). These chemical cues act as shared environmental drivers, causing both species to aggregate in regions where  $v_1$  enhances prey growth and simultaneously attracts predators. Likewise, areas with low chemical signal levels become unfavourable for both, leading to co-located minima. As a result, the dominant unstable mode in the Turing instability drives  $u_1, u_2, v_1,$  and  $v_2$  to vary in phase, producing synchronized predator–prey hotspots rather than spatially offset distributions typical of classical predator–prey interactions.

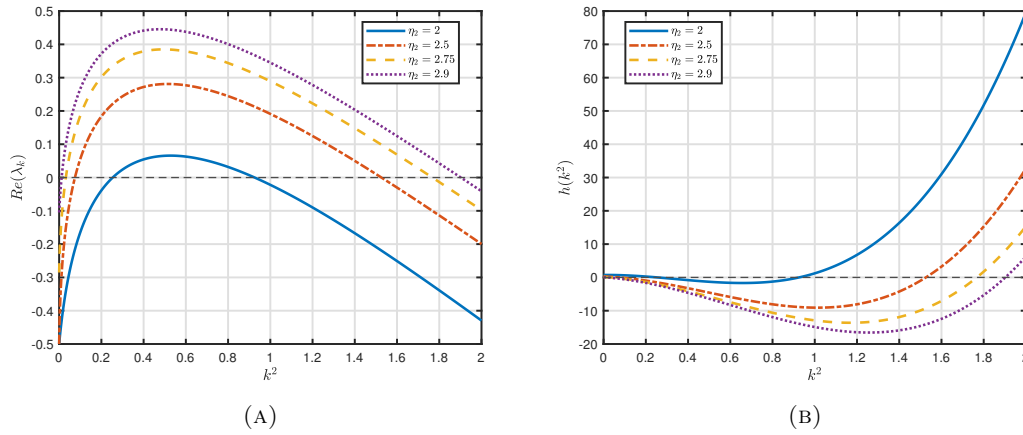


FIGURE 5. (a) Dispersion relation and (b)  $h(k^2)$  with respect to  $k^2$ , where  $d_{11} = 0.1, d_{12} = 1, d_3 = 3, d_{21} = 1, d_{22} = 2, d_4 = 2, \mu_1 = 2, \mu_2 = 3, \lambda_1 = 2, \lambda_2 = 1, a_1 = a_2 = b_1 = b_2 = 0.5, \eta_1 = 10$ .

TABLE 2. Comparative summary of Turing pattern formation under various parameter regimes.

Figure	Key Parameters Varied	Pattern Type (Predator & Prey)	Observations
6	$\eta_2 = 2, 2.25, 2.5$	Spot-Stripes $\rightarrow$ labyrinthine $\rightarrow$ localized spot-stripes.	Increasing predation rate ( $\eta_2$ ) reduces predator-prey spatial mixing. Predator aggregation becomes more localized, implying stronger prey avoidance and increased predator clustering around favourable patches.
7	$\eta_2 = 2.65, 2.75, 2.9$	localized spot-stripes $\rightarrow$ hexagonal spots.	Consistent with the first figure, we find that isolated coexistence spots emerge when $\eta_2 \approx \frac{\mu_2 \lambda_1}{\mu_1}$ .
8	$\eta_1 = 5, \eta_2 = 0.95$ and $\eta_1 = 10, \eta_2 = 0.25, 0.75$	Labyrinths / stripes-spots / spots.	Here, a higher $\eta_1$ promotes the formation of isolated coexistence spots.
9	Small $\mu_1, \mu_2, \lambda_1, \lambda_2$	Regular isolated hexagonal spot and dense square spot	An increase in $\eta_1$ leads to a transition from isolated coexistence spots to dense, square-shaped patches
10	$\eta_2 = 1, 1.5$	Labyrinths (lattice stripe) $\rightarrow$ refined stripes	Balanced growth and diffusion yield stable coexistence bands
11	Coefficients $d_{i,j}$	Disordered / irregular patterns	Cross-diffusion amplifies segregation scale but preserves predator-prey synchrony

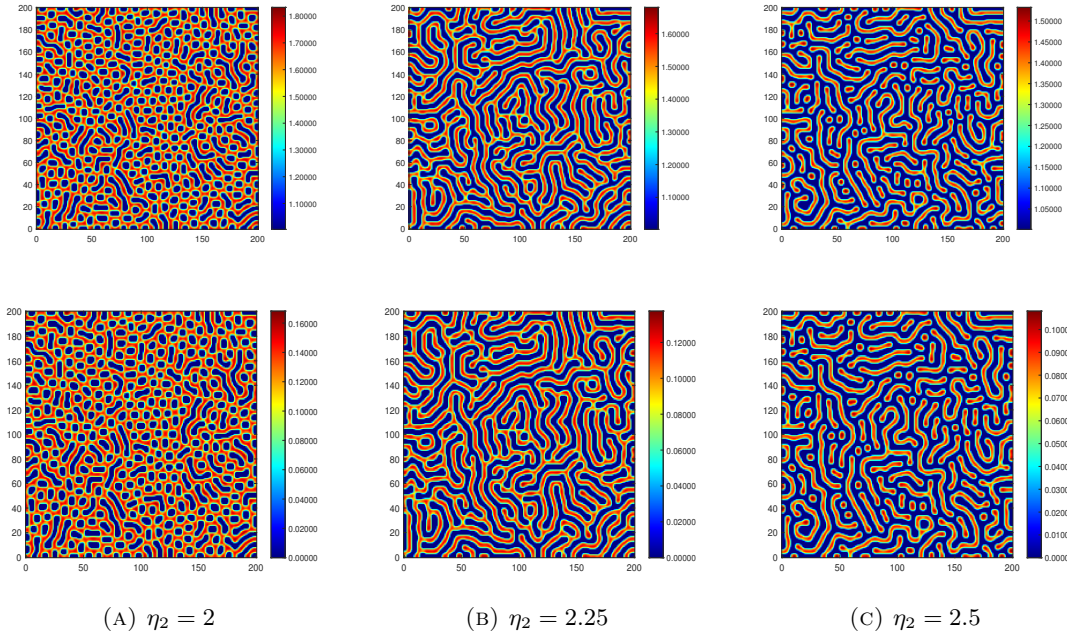


FIGURE 6. Spatial distributions of the species Predator  $u_1$  (first row) and Prey  $u_2$  (second row), where  $d_{11} = 0.1, d_{12} = 1, d_3 = 3, d_{21} = 1, d_{22} = 2, d_4 = 2, \mu_1 = 2, \mu_2 = 3, \lambda_1 = 2, \lambda_2 = 1, a_1 = a_2 = b_1 = b_2 = 0.5, \eta_1 = 10$ .

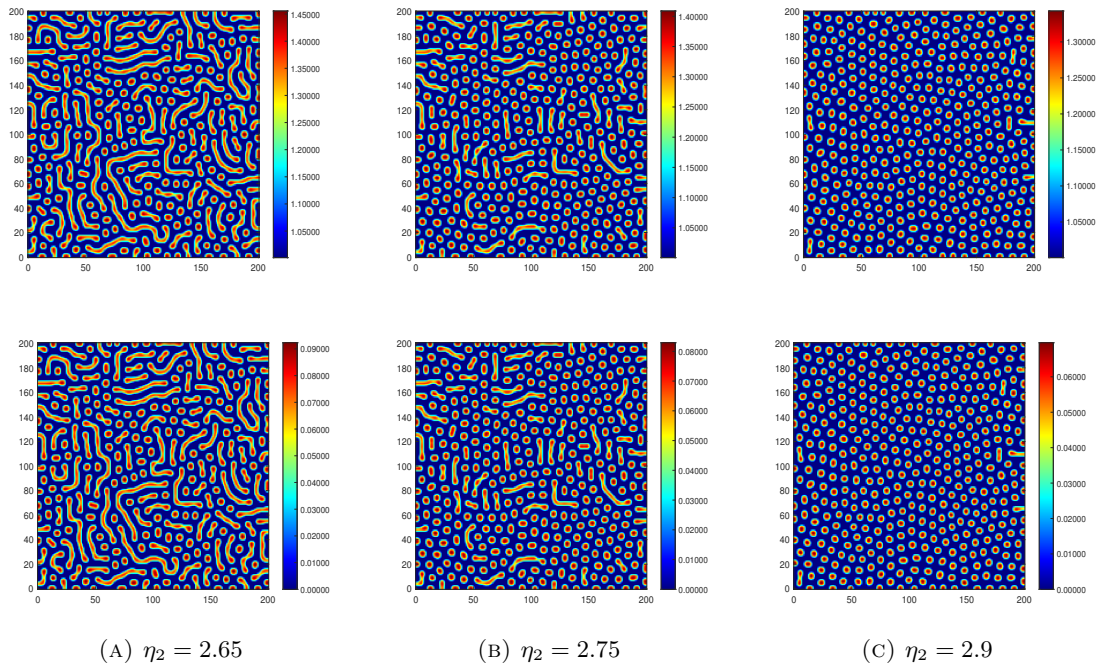


FIGURE 7. Spatial distributions of the species Predator  $u_1$  (first row) and Prey  $u_2$  (second row), where  $d_{11} = 0.1, d_{12} = 1, d_{21} = 1, d_{22} = 2, d_3 = 3, d_4 = 2, \mu_1 = 2, \mu_2 = 3, \lambda_1 = 2, \lambda_2 = 1, a_1 = a_2 = b_1 = b_2 = 0.5, \eta_1 = 10$ .

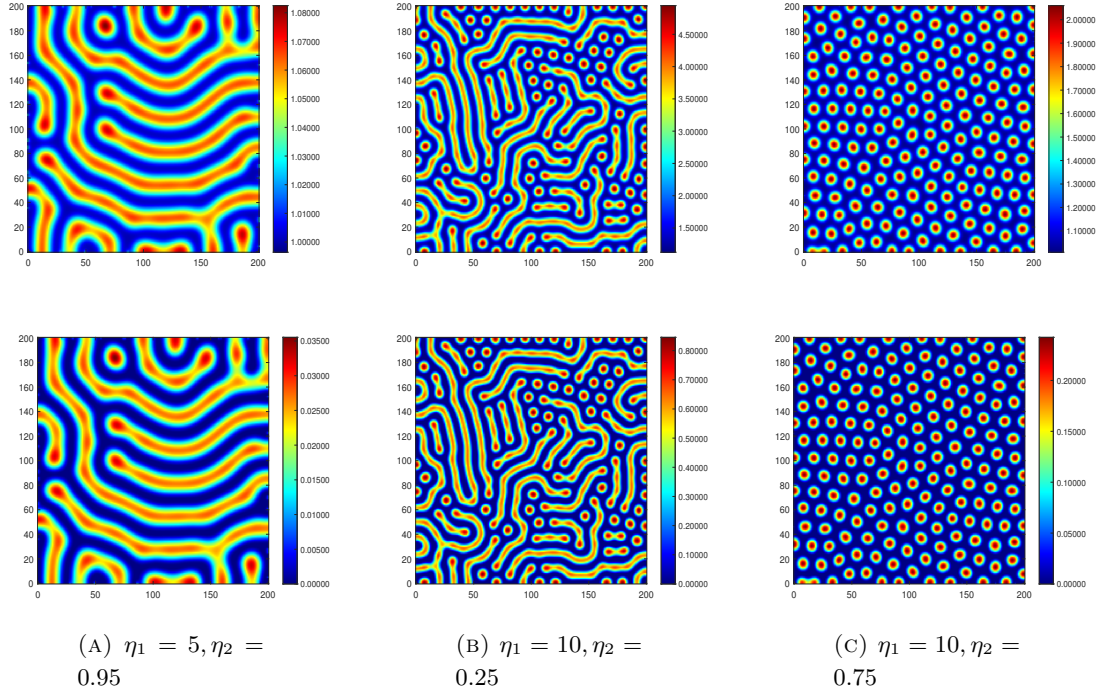


FIGURE 8. Spatial distributions of the species Predator  $u_1$  (first row) and Prey  $u_2$  (second row), where  $d_{11} = 3.25, d_{12} = 3, d_3 = 0.75, d_{21} = 5, d_{22} = 3, d_4 = 0.75, a_1 = a_2 = b_1 = b_2 = 0.5, \mu_1 = 2, \mu_2 = 1, \lambda_1 = 2, \lambda_2 = 1$ .

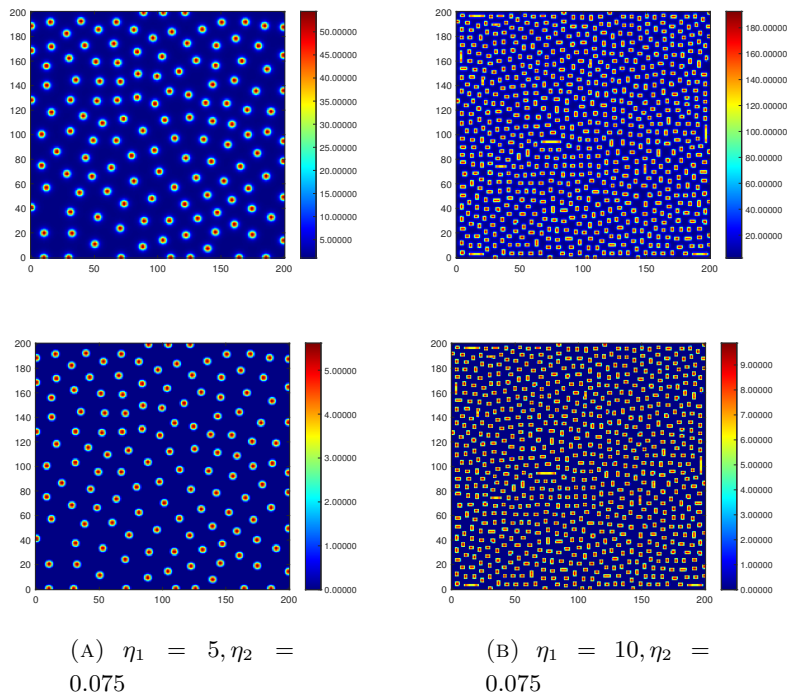


FIGURE 9. Spatial distributions of the species Predator  $u_1$  (first row) and Prey  $u_2$  (second row), where  $d_{11} = 3.25, d_{12} = 3, d_3 = 0.75, d_{21} = 5, d_{22} = 3, d_4 = 0.75, a_1 = a_2 = b_1 = b_2 = 0.5, \mu_1 = 0.5, \mu_2 = 0.1, \lambda_1 = 0.5, \lambda_2 = 0.1$ .

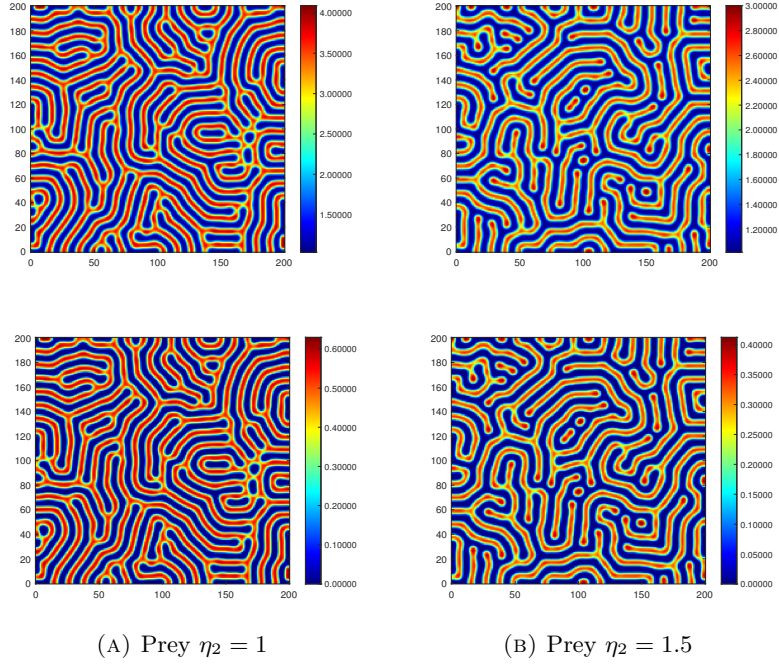


FIGURE 10. Spatial distributions of the species Predator  $u_1$  (first row) and Prey  $u_2$  (second row), where  $d_{11} = 1, d_{12} = 1, d_3 = 1, d_{21} = 5, d_{22} = 5, d_4 = 1.5, a_1 = a_2 = b_1 = b_2 = 0.5, \mu_1 = 2, \mu_2 = 3, \lambda_1 = 2, \lambda_2 = 1, \eta_1 = 10$ .

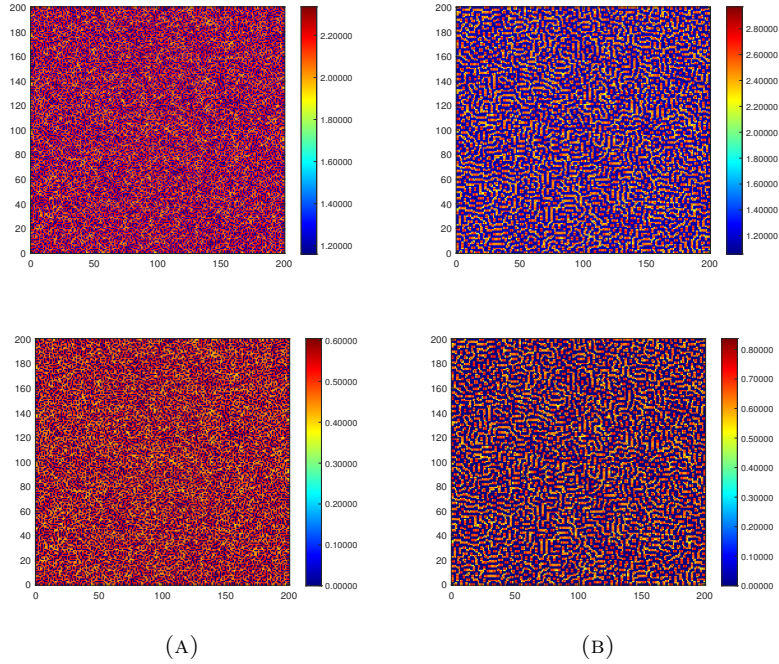


FIGURE 11. Spatial distributions of the species Predator  $u_1$  (first row) and Prey  $u_2$  (second row), where (a, c)  $d_{11} = 0.1, d_{12} = 1, d_{21} = 0.1, d_{22} = 1, d_3 = 3, d_4 = 3, \mu_1 = 2, \mu_2 = 3, \lambda_1 = 2, \lambda_2 = 1, a_1 = a_2 = b_1 = b_2 = 5, \eta_1 = 5, \eta_2 = 1.5$ . (b, d)  $d_{11} = 0.1, d_{12} = 1, d_{21} = 1, d_{22} = 2, d_3 = 3, d_4 = 2, \mu_1 = 2, \mu_2 = 3, \lambda_1 = 2, \lambda_2 = 1, a_1 = a_2 = b_1 = b_2 = 5, \eta_1 = 5, \eta_2 = 1.5$ .

## 7. DISCUSSIONS AND CONCLUSION

This study examined a predator–prey cross-diffusion system coupled with two chemical substances under homogeneous Neumann boundary conditions. Under suitable assumptions on the model parameters, the global existence of classical solutions bounded in the  $\mathcal{L}^\infty(\Omega)$  norm for  $n \geq 2$  established. Global asymptotic stability of the spatially homogeneous equilibria is derived by constructing an appropriate Lyapunov functional. The analysis leads to the following stability results with biological relevance:

- (i) If the predation rate  $\eta_2$  satisfies  $\eta_2 < \frac{\mu_2 \lambda_1}{\mu_1}$  and the cross-diffusion coefficients  $d_{12}^2$  and  $d_{22}^2$  are sufficiently small, the system admits a unique positive equilibrium that is globally asymptotically stable, implying long-term coexistence of prey and predator populations.
- (ii) If  $\eta_2 \geq \frac{\mu_2 \lambda_1}{\mu_1}$  and  $d_{12}^2$  is sufficiently small, the semi-trivial equilibrium becomes globally asymptotically stable, indicating eventual extinction of the prey population.

Beyond stability analysis, diffusion-driven instability and spatial pattern formation are also investigated. The results highlight the significant role of predation intensity in shaping spatial pattern formation in predator–prey systems mediated by two chemical substances. The spatial patterns obtained in Figures 6 - 11 reveal a rich spectrum of Turing-type structures arising from the interplay between self-diffusion, cross-diffusion and nonlinear predator–prey interactions. As the predation rate  $\eta_2$  increase (Figures 6 and 7), the system undergoes a clear transition from extended labyrinthine stripes to mixed stripe–spot formations and ultimately to highly ordered hexagonal spot arrays, indicating that stronger prey self-enhancement favours localized aggregation and sharp spatial segregation. Variations in both  $\eta_1$  and  $\eta_2$  (Figure 8) demonstrate that the balance between predator activation and prey response strongly shapes pattern geometry: moderate  $\eta_1$  supports broad, continuous stripe networks, whereas higher  $\eta_1$  produces dense spot patterns corresponding to isolated predator territories. Extremely small  $\mu_1, \mu_2, \lambda_1, \lambda_2$  and  $\eta_2$  (Figure 9) generate fine-grained spot microstructures, reflecting highly fragmented ecological niches and reduced spatial coherence. When  $\eta_2$  is moderately increased (Figure 10), stripe patterns become more refined and regularly spaced, indicative of stable predator movement corridors aligned with prey availability. Finally, under mixed diffusion configurations (Figure 11), the system loses structural organization and exhibits irregular, noise-like textures, suggesting parameter regimes near the boundaries of Turing instability where no dominant spatial wavelength emerges. Collectively, these patterns demonstrate how subtle adjustments in biological interaction strengths and diffusion parameters can shift ecosystems between coherent territorial structures, localized resource patches and disordered distributions.

## ACKNOWLEDGMENTS

GS and JS thank the Anusandhan National Research Foundation (ANRF), formerly Science and Engineering Research Board (SERB), Govt. of India for their support through Core Research Grant (CRG/2023/001483) during this work.

## REFERENCES

- [1] A.J. Lotka, *Elements of Physical Biology*, Williams & Wilkins, New York, 1925.
- [2] V. Volterra, *Variazioni e fluttuazioni del numero d'individui in specie animali conviventi*, volume 2, Societa anonima tipografica “Leonardo da Vinci” (1927).
- [3] A.M. Turing, The chemical basis of morphogenesis, *Trans. R. Soc. Lond.*, B237 (1952), 37-72.

- [4] L.A. Segel and J.L. Jackson, Dissipative structure: an ecological example, *J. Theor. Biol.*, 37 (1972), 545-559.
- [5] J. Chattopadhyay, P.K. Tapaswi, D. Datta, D. Chattopadhyay, Formation of a dissipative structure: A nonlinear analysis, *Ecol. Model.*, 73 (1994), 205-214.
- [6] J.F. McLaughlin, J. Roughgarden, Predation across spatial scales in heterogeneous environments, *Theor. Popul. Biol.*, 41 (1992), 277-299.
- [7] N. Ahmed, M.W. Yasin, A. Akgül, D. Baleanu, O. Tintareanu-Mircea, Mathematical analysis and pattern formation in diffusive predator-prey system, *J. Appl. Math. Comput.*, 71 (2025), 3037-3058.
- [8] L.N. Guin, S. Acharya, Dynamic behaviour of a reaction-diffusion predator-prey model with both refuge and harvesting, *Nonlinear Dyn.*, 88 (2017), 1501-1533.
- [9] M.E. Gurtin, Some mathematical models for population dynamics that lead to segregation, *Q. J. Appl. Math.*, 32 (1974), 1-8.
- [10] G. Hu, X. Li, Y. Wang, Pattern formation and spatiotemporal chaos in a reaction-diffusion predator-prey system, *Nonlinear Dyn.*, 81 (2015), 265-275.
- [11] A. Okubo, *Diffusion and Ecological Problems: Mathematical Models*. Biomathematics, Vol. 10. Springer, Berlin. (1980).
- [12] G.Q. Sun, J. Zhang, L.P. Song, Z. Jin, B.L. Li, Pattern formation of a spatial predator-prey system, *Appl. Math. Comput.*, 218 (2012), 11151-11162.
- [13] V. Tiwari, J.P. Tripathi, D. Jana, S.K. Tiwari, R.K. Upadhyay, Exploring complex dynamics of spatial predator-prey system: role of predator interference and additional food, *Int. J. Bifurcat. Chaos.*, 30 (2020), 2050102.
- [14] S. Raychaudhuri, D.K. Sinha, J. Chattopadhyay, Effect of time-varying cross-diffusivity in a two-species Lotka-Volterra competitive system, *Ecol. Model.*, 92 (1996), 55-64.
- [15] R.K. Upadhyay, A. Patra, B. Dubey, N.K. Thakur, A predator-prey interaction model with self-and cross-diffusion in aquatic systems, *J. Biol. Syst.*, 22 (2014), 1-22.
- [16] S. Ghorai, S. Poria, Pattern formation and control of spatiotemporal chaos in a reaction diffusion prey-predator system supplying additional food, *Chaos Solitons Fractals*, 85 (2016), 57-67.
- [17] Q. Cao, J. Wu, Pattern formation of reaction-diffusion system with chemotaxis terms, *Chaos*, 31 (2021), 113118.
- [18] B.T. Mbopda, S. Issa, S. Abdoukary, R. Guiem, H.P. Fouda, Pattern formations in nonlinear dynamics of hepatitis B virus, *Eur. Phys. J. Plus*, 136 (2021), 586.
- [19] S. Ghorai, O. Umut, S. Poria, Analysis of patterns in an additional food-provided predator-prey reaction diffusion model using amplitude equations, *Pramana J. Phys.*, 97 (2023), 200.
- [20] Y. Wang, X. Zhou, W. Jiang, Bifurcations in a diffusive predator-prey system with linear harvesting, *Chaos Solitons Fractals*, 169 (2023), 113286.
- [21] B. Chakraborty, S. Marick, N. Bairagi, Diffusion-driven instabilities in a tri-trophic food web model: From Turing to non-Turing patterns and waves, *Chaos Solitons Fractals*, 189 (2024), 115634.
- [22] G. Mandal, L.N. Guin, S. Chakravarty, Complex patterns in a reaction-diffusion system with fear and anti-predator responses, *Int. J. Bifurcat. Chaos.*, 34 (2024), 2450154.
- [23] S. Li, W. Jiang, X. Zhang, J. Wang, Dynamic analysis, patterns formation and numerical simulation of a reaction-diffusion system, *Nonlinear Dyn.*, 113 (2025), 4923-4947.
- [24] L.T. Bhutia, S. Biswas, E. Das, T.K. Kar, B. Bhunia, Evolution of Turing patterns of a predator-prey system with variable carrying capacity and harvesting, *Chaos Solitons Fractals*, 191 (2025), 115790.
- [25] E. Das, T.K. Kar, L.T. Bhutia, S. Biswas, B. Bhunia, Asymptotic and transient approaches of harvested predator-prey models with reaction-diffusion, *Eur. Phys. J. Plus*, 140 (2025), 310.
- [26] G. Mandal, L.N. Guin, S. Chakravarty, Cross-diffusion-induced instabilities in a cooperative hunting population with Allee effect, *Eur. Phys. J. Plus*, 140 (2025), 96.
- [27] P.J. Pal, D. Biswas, T. Saha, Spatial dynamics and pattern formation in fragmented habitats: A study using a diffusive Bazykin model with Allee effect, *Chaos Solitons Fractals*, 192 (2025), 116043.
- [28] M.W. Yasin, N. Ahmed, A. Akgül, M.Z. Baber, D. Baleanu, O. Tintareanu-Mircea, Spatio-temporal patterns and Turing-Hopf bifurcation in a spatially extended prey-predator model with ratio-dependent interactions, *Model. Earth Syst. Environ.*, 11 (2025), 219.
- [29] S. Majee, S. Jana, J. Ramprabhakar, Complex spatiotemporal dynamics in an eco-epidemic model: Turing instability, non-stationary patterns and chaos control, *Math. Comput. Simul.*, 240 (2026), 650-667.
- [30] J.D. Murray, *Mathematical Biology I: An Introduction*, Springer-Verlag, New York, 2002.

- [31] J.D. Murray, *Mathematical Biology II: Spatial Models and Biomedical Applications*, Springer-Verlag, New York, 2003.
- [32] S.T. Abedon, *Bacteriophage Ecology: Population Growth, Evolution and Impact of Bacterial Viruses*, Cambridge University Press, 2009.
- [33] J.S. Weitz, T. Poisot, J.R. Meyer, C.O. Flores, S. Valverde, M.B. Sullivan, M.E. Hochberg, Phage-bacteria infection networks, *Trends Microbiol.*, 21 (2013), 82–91.
- [34] D.C.O. Thornton, Dissolved organic matter (DOM) release by phytoplankton in the contemporary and future ocean, *Eur. J. Phycol.*, 49 (2014), 20–46.
- [35] L. Jiang, O.M.E. Schofield, P.G. Falkowski, Adaptive evolution of phytoplankton cell size, *Am. Nat.*, 166 (2005), 496–505.
- [36] H. Amann, Nonhomogeneous linear and quasilinear elliptic and parabolic boundary value problems, *Function Spaces, Differential Operators and Nonlinear Analysis*, 133 (1993), 9–126.
- [37] J. Zheng, Boundedness of solutions to a quasilinear parabolic-elliptic Keller-Segel system with logistic source, *J. Differ. Equ.*, 259 (2015), 120–140.
- [38] S. Gnanasekaran, N. Nithyadevi, C. Udhayashankar, Global existence and asymptotic behavior of a predator-prey chemotaxis system with inter-species interaction coefficients, *J. Differ. Equ.*, 378 (2024), 264–302.
- [39] X. Cao, Boundedness in a quasilinear parabolic-parabolic Keller-Segel system with logistic source, *J. Math. Anal. Appl.*, 412 (2014), 181–188.
- [40] M. Hieber, J. Prüss, Heat kernels and maximal  $\mathcal{L}^q(\Omega)$ - $\mathcal{L}^p(\Omega)$  estimate for parabolic evolution equations, *Commun. Partial Differ. Equ.*, 22 (1997), 1647–1669.
- [41] O. Ladyzenskaja, V. Solonnikov, N. Uralceva, *Linear and quasi-linear equations of parabolic type*, American Mathematical Society, 1968.
- [42] H. Amann, *Linear and Quasilinear Parabolic Problems: Volume I, Abstract Linear Theory*, Birkhäuser Verlag, Basel, (1995).
- [43] Y. Tao, M. Winkler, Boundedness in a quasilinear parabolic-parabolic Keller-Segel system with subcritical sensitivity, *J. Differ. Equ.*, 252 (2012), 692–715.
- [44] X. Bai, M. Winkler, Equilibration in a fully parabolic two-species chemotaxis system with competitive kinetics, *Indiana Univ. Math. J.*, 65 (2016), 553–583.
- [45] M. Wang, A diffusive logistic equation with a free boundary and sign-changing coefficient in time-periodic environment, *J. Funct. Anal.*, 270 (2016), 483–508.
- [46] J. Wang, M. Wang, The diffusive Beddington-DeAngelis predator-prey model with nonlinear prey-taxis and free boundary, *Math. Methods Appl. Sci.*, 41 (2018), 6741–6762.
- [47] T. Li, A. Suen, M. Winkler, C. Xue, Global small-data solutions of a two-dimensional chemotaxis system with rotational flux terms, *Math. Models Methods Appl. Sci.*, 25 (2015), 721–746.
- [48] M.M. Porzio, V. Vespi, Holder estimates for local solutions of some doubly nonlinear degenerate parabolic equations, *J. Differ. Equ.*, 103 (1993), 146–178.

(GS) DEPARTMENT OF MATHEMATICS, NATIONAL INSTITUTE OF TECHNOLOGY TIRUCHIRAPPALLI, TAMILNADU 620015, INDIA

*Email address:* `sekaran@nitt.edu`

(JS) DEPARTMENT OF MATHEMATICS, NATIONAL INSTITUTE OF TECHNOLOGY TIRUCHIRAPPALLI, TAMILNADU 620015, INDIA

*Email address:* `jitraj@nitt.edu`

(ODM) FACULTY OF MILITARY SCIENCE, STELLENBOSCH UNIVERSITY, STELLENBOSCH, SOUTH AFRICA

*Email address:* `makinded@gmail.com`

(JC) AGRICULTURAL & ECOLOGICAL RESEARCH UNIT, INDIAN STATISTICAL INSTITUTE KOLKATA, WEST BENGAL 700108, INDIA

*Email address:* `joydev@isical.ac.in`